2018

Adapting a Field-Deployable Noble Gas Mass Spectrometer for Continuous Measurements of Helium

Katherine Chan
kchan5@wellesley.edu

Adapting a Field-Deployable Noble Gas Mass Spectrometer for Continuous Measurements of Helium

Katherine Chan
Advisor: Professor Rachel H.R. Stanley
Department of Chemistry, Wellesley College

Submitted in Partial Fulfillment of the Prerequisite for Honors in Chemical Physics
April 2018

Acknowledgments

First, I would like to thank my advisor, Professor Rachel Stanley. When I joined your lab as a first year, I wasn't sure what doing research meant let alone whether I wanted to do research as a career. Now, as a graduating senior, I'm off to graduate school ready and excited to start my career in research, and I owe it all to you. Thank you for all of your guidance and support throughout my time at Wellesley. The mentorship I've had the privilege of receiving from you will be something I will cherish in graduate school and beyond. Your positivity in the face of adversity and your inspiring outlook on life are things I will always admire. This thesis would have been so much harder without it. I hope to one day achieve even a fraction of your confidence and optimism in both research and in life. I feel so lucky to have had you as my advisor.

I would also like to thank my thesis committee members: Professor Chris Arumainayagam and Professor James Battat. Thank you both for your expertise in vacuum chambers and Chris for your much-appreciated help with trouble-shooting our mass spectrometer. To Chris, I am so very indebted to you for so many of the opportunities I've had at my time at Wellesley. Thank you so much for believing in me and supporting my endeavors when they seemed unlikely to succeed. My experience at Wellesley would be so different without you and I don't think there are words to express how grateful I am. To James, it's been so great getting to know you this past year as part of my thesis and in PHYS 310. PHYS 310 has been one of my favorite experiences at Wellesley. It's been such a treat getting to apply all of the concepts I've learned only in theory and to be able to do that under the guidance of you and Jerome. I can see the hard work and passion you invest in the class and I appreciate it so much. Thank you so much for your patience, good humor, and dedication.

I would also like to recognize Professor Philip Hirschhorn for agreeing to be the honors visitor of my thesis committee. Thank you for being the inspiration for my initial foray into proof-based mathematics and for being so understanding when I decided that was not for me. Thank you also for your humor, peanut butter crackers (and occasional Halloween candy), and for letting me chat with you way past your office hours even though I haven't taken a class with you since first year.

Thank you also to my fellow lab members (present: Brenda Ji '18, Callie Krevanko '18, Marissa Menzel '18, Lumi Kinjo '19, Helene Alt DS '19, Elizabeth Lambert '20, Dani Aldrett '21 and past: Alice Zhou '17, Elle Friedberg '17, and Oana Diaconescu '15) in the Stanley lab for your encouragement and support. To my thesis t(wednesdays) group, Brenda Ji, Lorrie He, Elisa Wang, and Angel Kuo, thank you for the lively company during the long nights in Sage Lounge, sharing in the glow of successes, commiserating with failures, and believing in me when I didn't believe in myself. To More Friends, thank you for all of the support and all of the amazing times we've shared. I'm so proud of all of you and all that you've accomplished and persevered through this year, and I'm so excited to see what you accomplish after we leave Wellesley.

Finally, thank you to my amazing family who has supported me every step of the way. Thank you for keeping things in perspective, having faith in me, and supporting me in everything I've wanted to do. I will always be grateful for the sacrifices you've made to make sure I have the widest range of opportunities possible. None of this would be possible without you.

Table of Contents

Abstract

Isotopes of the five stable noble gases (He, Ne, Ar, Kr, and Xe) are useful in analyzing physical processes in the environment such as air-sea gas exchange and sea ice formation and melting. Traditional measurements of noble gases are costly and time-consuming because of the need to transport water samples to analyze in a laboratory-based mass spectrometer. Field deployable mass spectrometers were developed as a low-cost method to increase the temporal resolution of the measurements. Our system utilizes a quadrupole mass spectrometer in tandem with a gas equilibrator cartridge to continuously measure equilibrated gases from water with ambient air as a calibration standard. The reproducibility of the system is better than 0.7% for all gas ratios in a lab environment. However, our current configuration is not optimized for measuring helium because of the high permeability of helium through many of the materials used. Nonetheless, measuring helium will yield insight into quantifying bubble processes, which significantly affects rates of air-sea gas exchange. Our mass spectrometer configuration was thus extended to measure helium by switching from fused silica capillaries to stainless steel capillaries and switching from Tygon tubing to Viton tubing. The equilibration and precision of the new system was compared to that of the old configuration. Leak tests were performed on the old and new configuration to assess whether the leakiness of the system has improved. Results showed effective measurements of He with precisions better than 0.80% for both He/Ar and He/Kr at water temperatures of 22°C and above. Further optimization is needed to improve the equilibration of He and Ne at water temperatures of 10°C.

Chapter 1: Introduction

1. Characteristics of Noble Gases

Noble gases are characterized by filled outer valence shells, making them stable in their elemental form and unlikely to form chemical compounds at standard conditions on Earth[1]. As a result, the behavior of noble gases in nature is largely dictated by physical processes that are well-understood such as diffusion, phase partitioning, and nuclear transformations.[2] Because noble gases are biologically and chemically inert and thus respond mostly to physical forcings, they are widely used as environmental tracers of physical processes. Noble gas tracers are advantageous in particular because the five stable noble gases (He, Ne, Ar, Kr, Xe) vary widely in solubility and diffusivity.[3] As illustrated in Figure 1, the molecular diffusivity of the noble gases increases linearly with temperature and inversely relates to atomic mass such that helium is the most diffusive.[4] In contrast, solubility decreases non-linearly with temperature for the heavier noble gases and is largely unaffected by temperature for helium and neon.[4] The range of the molecular diffusivities varies by a factor of 7 over a temperature range of 5-35°C in pure water while solubility varies by over an order of magnitude.[4-5] This range of physical properties allows for the decoupling of physical processes and the ability to quantify them separately.[6] In particular, noble gases are being used in seawater because they have well-known sources and sinks.[3] Currently, noble gas tracers are being used to study physical processes such as air-sea gas exchange and glacial melting and formation.[4]

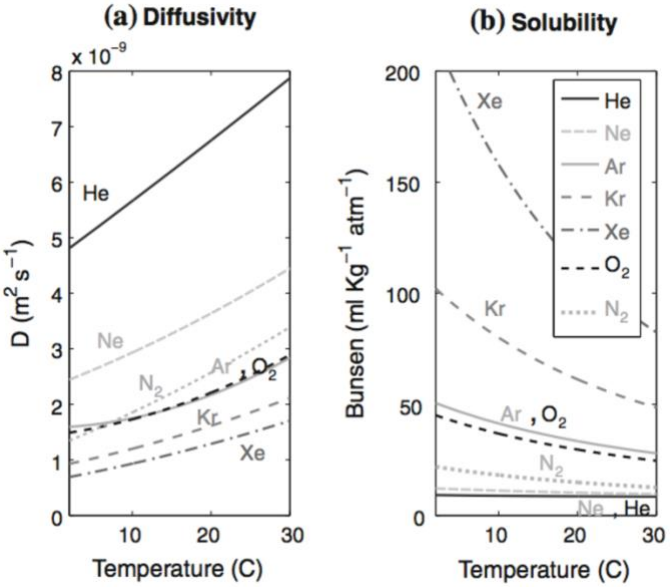

Figure 1: (a) Molecular diffusivities of the five noble gases, oxygen, and nitrogen as a function of temperature. (b) Solubility of the noble gases, oxygen, and nitrogen in seawater as a function of temperature. Figure reproduced from Stanley and Jenkins (2013)[4]

1.1 Sources of Noble Gases in Seawater

The physical processes for which noble gas tracers are useful in seawater depend on the geochemical channels by which they enter and exit the water. Sources of noble gases in water are divided into two categories: atmospheric sources and non-atmospheric sources.[7] Atmospheric sources are the main contributor of noble gases in seawater.[7]

1.2 Atmospheric Noble Gases

Atmospheric noble gases enter the water largely through air-sea gas exchange. Because gas exchange processes occur relatively quickly, the noble gases in surface waters are often effectively at equilibrium with the atmosphere in amounts that are proportional to the partial pressure of the noble gas according to Henry's Law:

$$p_i = H_i C_i \tag{1}$$

$$i = He, Ne, Ar, Kr, Xe$$

where p_i is the partial pressure of the noble gas, i , H_i is the Henry coefficient which is expressed as a function of salinity and temperature, and C_i is the equilibrium concentration of the noble gas, i , in water.[4, 7-8] Over the timescales relevant to gas exchange processes, it can be assumed that the noble gas compositions of the atmosphere are constant.[8] This assumption allows for the expression of the partial pressure of the noble gases in terms of the total atmospheric pressure (p_{tot}):

$$p_i = z_i[p_{tot} - e_w(t)] \quad (2)$$

where z_i, the volume or mole fraction of the gas, and e_w(T), the water vapor content, are modifications to the total atmospheric pressure.[3]

1.2.1 Deviations from Henry's Law

Deviations from Henry's law can occur due to physical processes such as rapid temperature changes, ice formation or melting, and bubble effects.[4] As a result, noble gases are especially useful in studying these physical processes because information about the processes can be obtained by analyzing the saturation anomalies (Δ), the difference between observed and expected gas concentration, expressed as:

$$\Delta = \left(\frac{c_{obs}}{c_0} - 1\right) * 100\% \quad (3)$$

where c_{obs} is the observed gas concentration and c_0 is the equilibrium gas concentration.[9] In this section, bubble effects and ice melting and formation will be discussed to illustrate the exploitation of saturation anomalies to trace physical processes.

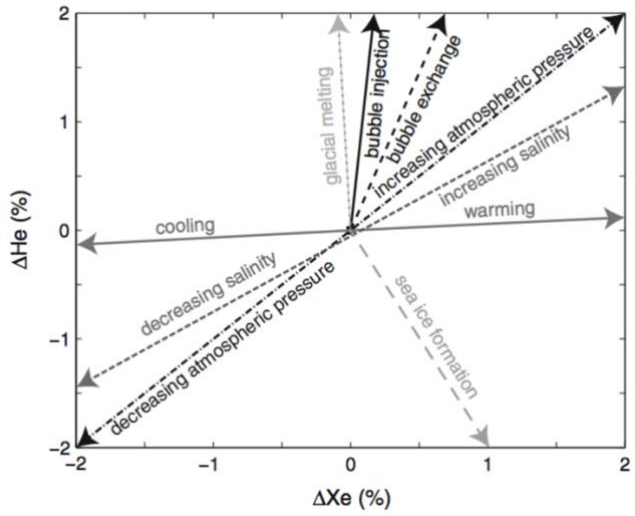

Figure 2: Schematic illustrating the effect of various physical processes on the saturation anomalies of He and Xe. Figure reproduced from Stanley and Jenkins (2013)[4]

1.2.3 Bubble Processes

Bubble processes can result in deviations from equilibrium concentrations and have significant implications in quantifying air-sea gas exchange fluxes. Bubbles are formed when waves break at the ocean surface and subsequently, penetrate deeper into the ocean through turbulence.[10-12] In particular, bubbles have the greatest impact on air-sea gas exchange rates at high wind speeds because of the greater incidence of bubbles.[11, 13] The sizes of these bubbles may change in responses to changes in amounts of gas and ambient pressure.[11] Smaller bubbles travel to lower depths and dissolve completely, in a process known as "air injection." [3] Air injection has a larger effect on less soluble gases because less soluble gases have low concentrations in water. Small bubbles then tend to preferentially increase the amount of insoluble gases.[14-15] The saturation anomaly thus is inversely proportional to the equilibrium concentrations of the gases.[3, 13]. In contrast, larger bubbles partially dissolve, rise due to their faster buoyant rising, and burst at the ocean surface.[11, 16] As a result, large bubbles increase the amount of less soluble gases to a lesser extent than smaller bubbles. Thus, bubble processes tend to affect He and Ne the most as they are both slightly soluble. [13]

Bubbles impact air-sea gas exchange through two processes. Due to hydrostatic pressure and surface tension, bubbles tend to compress, and the partial pressure of gases inside the bubble is greater than those outside.[17] Because of this pressure difference, bubbles release gases into the ocean even if the seawater is already supersaturated.[11] This has the effect of increasing the diffusion rate of gases from the ocean to the atmosphere and is referred to as the "equilibrium bubble effect".[11] The second effect is called the kinetic bubble effect and describes the additional air-sea gas exchange channel produced by bubbles that allows faster equilibration of gases into the ocean.[11] Together, these two processes increase the air-sea gas exchange rate and result in a slight supersaturation of gases in seawater.

Because of the breadth of physical properties spanned by the noble gases, noble gas tracers are being used to study the impact of bubbles on air-sea gas exchange. Noble gases are particularly useful in separating the contribution of gases by bubble processes and diffusive gas exchange, the latter of which refers to gas exchange across the rough surface of the air-sea interface.[13, 15, 18] As discussed earlier, He and Ne are the most sensitive to bubble processes, while Ar, Kr, and Xe are more sensitive to diffusive gas exchange because of their higher solubility and highly temperature dependent solubility.[4] Thus, using all five stable noble gases allows for improved constraints in calculating the flux of diffusive gas exchange and air injection.[13]

1.2.4 Sea Ice Formation and Melting

Noble gas tracers and their saturation anomalies caused by the melting and formation of ice have also proved useful in studying ice-water interfaces. The formation of ice causes supersaturations of the heavier noble gases in the remaining water because they are excluded from the ice lattice as water freezes.[19] In contrast, He and Ne tend to be undersaturated in the

water because their greater solubility in ice and their low solubility in water causes a large degree of partitioning between bubbles at the water-ice interface.[19] In turn, the increased solubility of He and Ne in ice results in supersaturations of these lighter noble gases when ice melts.[19] This property of He and Ne make those gases especially useful as water mass tracers in environments impacted by glacial melt. However, glacial meltwater produces a similar excess saturation of He and Ne to that caused by bubble processes at high wind speeds. [20] Thus, additional tracers, such as the other noble gases, should be used in order to decouple and characterize the flux of glacial meltwater from that caused by bubbles.[20]

Recent studies have focused on using noble gas tracers to study ice shelf meltwater because of the role of ice shelves in mitigating the flux of glacial ice into the sea and subsequent melting.[20-21] In one of its earliest uses as a water mass tracer, the oversaturation of He in meltwater was used to study ice shelf meltwater.[22] To do so, the excess of ^{4}He relative to solubility equilibrium concentrations was calculated and used to estimate the fraction of meltwater in ice shelf water to quantify the extent of ice shelf melting.[22]

1.3 Non-Atmospheric Noble Gases

Although physical processes such as injected air explain the supersaturation of dissolved gases in the ocean, one-third of the saturation anomaly for He is not accounted for by these physical processes. [3, 8] Investigations into the extra saturation anomaly have found that it is produced by non-conservative, non-atmospheric sources.[3] Non-atmospheric sources of noble gases include radiogenic and terrigenic sources.

1.3.1 Radiogenic Noble Gases

Radiogenic noble gases refer to noble gas isotopes that are produced by the decay of radioactive nuclides in rocks and minerals.[8, 23] Radioactive decay only substantially produces ^{3}He and ^{4}He from the alpha decay of ^{238}U, ^{235}U and ^{232}Th. However, ^{3}He can also be produced by the

radioactive decay of atmospheric tritium.[8] In aqueous environments, helium tends to accumulate if it is not directly exchanging with the atmosphere because of its low solubility, high diffusivity, and high mobility.[8] As a result, radiogenic helium isotopes are useful in quantifying the time elapsed since gas exchange at the surface, which is related to the water residence time.[8] Thus, analyzing helium isotopes in water allows determination of the water residence times and quantifies mixing rates and deep sea exchange. [24-25]

1.3.2 Terrigenic Noble Gases

Terrigenic noble gases refer to noble gases that are injected from Earth's crust and mantle.[8] Heavier helium isotopes are generated in Earth's crust through radioactive decay and are subsequently injected into seawater.[8] In Earth's mantle, lighter isotopes of helium dominate and originate from processes during Earth's formation.[26] The ratio of $^{3}He/^{4}He$ of a fluid is thus characteristic of the geochemical reservoir in which the fluid originated. [27] By measuring the helium isotope ratio in aquatic environments, the flux of fluids from Earth's lithosphere can be determined. [28] For instance, recent research has utilized helium isotope and noble gas ratios to investigate the origins of methane gas seepages from ocean sediments. [28-29]

1.4 Analytical Techniques in Measuring Noble Gases

Although noble gas tracers have become more prevalent over the past decade, they are still less frequently utilized than other isotope tracers such as the stable isotopes of water or radiocarbon. [30] A large reason for the less frequent application of noble gas tracers is that the analytical techniques used to measure noble gases tend to be complex.[30] Analyzing noble gases in aqueous samples is usually performed with mass spectrometry. As a result, noble gases must be extracted from liquid samples and then purified since the noble gases are present in very low amounts in aqueous systems. [1]

Traditional noble gas measurements are performed with discrete samples in a lab-based mass spectrometer. In lab-based configurations, gas extraction is commonly done by taking advantage of the low solubility of the noble gases that causes them to preferentially partition into the headspace above a liquid.[1] Liquid samples are collected in copper tubes, stainless steel tubes, or in evacuated glass bottles. [31-33] The samples are subsequently attached to an ultra-high vacuum (UHV) line to extract the liquid into a degassing chamber to allow for equilibration of the gases into the headspace.[25] Purification is commonly done by using "getters," active metal surfaces that remove abundant gases, cryogenic traps that captures gases at low temperatures (<10 K) and then selectively releases them one at a time, or a combination of the two. [1, 32, 34] Currently, most noble gas mass spectrometer configurations use an electron impact source, a quadrupole mass analyzer, and detection with a combination of secondary electron multipliers (SEM) and Faraday cups.[1] However, conducting noble gas measurements with lab-based mass spectrometers is time-consuming because analysis takes multiple hours per sample and samples need to be transported to laboratories. [35] Moreover, the equipment required to collect highly precise and accurate data is expensive. As a result, few laboratories are able to measure He, Ne, Kr, and Xe with high precision and accuracy.

Because of the costs and time associated with laboratory-based measurements, field-deployable noble gas mass spectrometers were developed to increase the spatial and temporal resolution of measurements. In contrast to laboratory-based measurements, field-deployable mass spectrometers can measure continuously by pumping water directly through the equilibration component of the system while constantly extracting and analyzing the gases. The continuous configuration reduces the processing time to several minutes per measurement at the cost of lower precision than traditional analytical methods. To extract gases, field-deployable

mass spectrometers commonly utilize one of two methods: a membrane contractor cartridge or a membrane inlet mass spectrometer (MIMS) system. A membrane contractor cartridge uses a gas permeable membrane to allow gases to equilibrate out of the liquid samples and into the headspace of the cartridge.[35] The MIMS system extracts gases by allowing gases to diffuse across a semi-permeable membrane, thereby eliminating the time needed for headspace equilibration. [36] Similar to lab-based systems, purification is done using getters and traps, although field-deployable systems may use dry ice traps at -80°C instead of cryogenic traps to remove water vapor. [35, 37] Additionally, field-deployable systems often use a quadrupole mass spectrometer because their smaller size and increased robustness compared to magnetic sector mass spectrometers makes them better suited for field studies. [36] Thus, field-deployable mass analysis can increase sample throughput of noble gas measurements at lower costs and labor intensity than traditional methods.

The Stanley lab's field-deployable mass spectrometer system has achieved accuracies of 1% or better for all ratios of Ne, Ar, Kr, and Xe.[35] However, our system is not configured to measure He because He permeates through most types of glass and potentially through other materials that make up our system. Mächler et al. developed a continuous field-deployable mass spectrometer that measures all five noble gases with an average overall error of 3% for He in the field, but they do not explicitly state whether He leak tests were done for the system. [38] Visser et al. conducted He leak experiments and improved the gas-tightness of their samples, but their system operated in discrete mode and yielded a precision of 2.1%. [37] This thesis describes the adaptation of our current continuous field-deployable mass spectrometer system to measure He. The findings of this project will be directly applied this summer to our experiments investigating the effects of bubbles on air-sea gas exchange at the University of Miami's SUrge STructure

Atmosphere INteraction (SUSTAIN) Facility, a novel wind-wave tank able to simulate a variety of wind and wave conditions. Improved helium measurements could also be useful in quantifying the input of oxygen into groundwater through excess air injection. [39] The following sections of this thesis will detail changes made to the system, subsequent leak tests, tests of the precision and accuracy of the new system and attempts to improve equilibration of the noble gases with the new system.

Chapter 2: Methods

2.1: Instrument Configuration

Experiments and modifications were performed on the gas equilibration mass spectrometer (GEMS) system described by Manning, et al. [35]. A schematic of the system is illustrated in Figure 3.

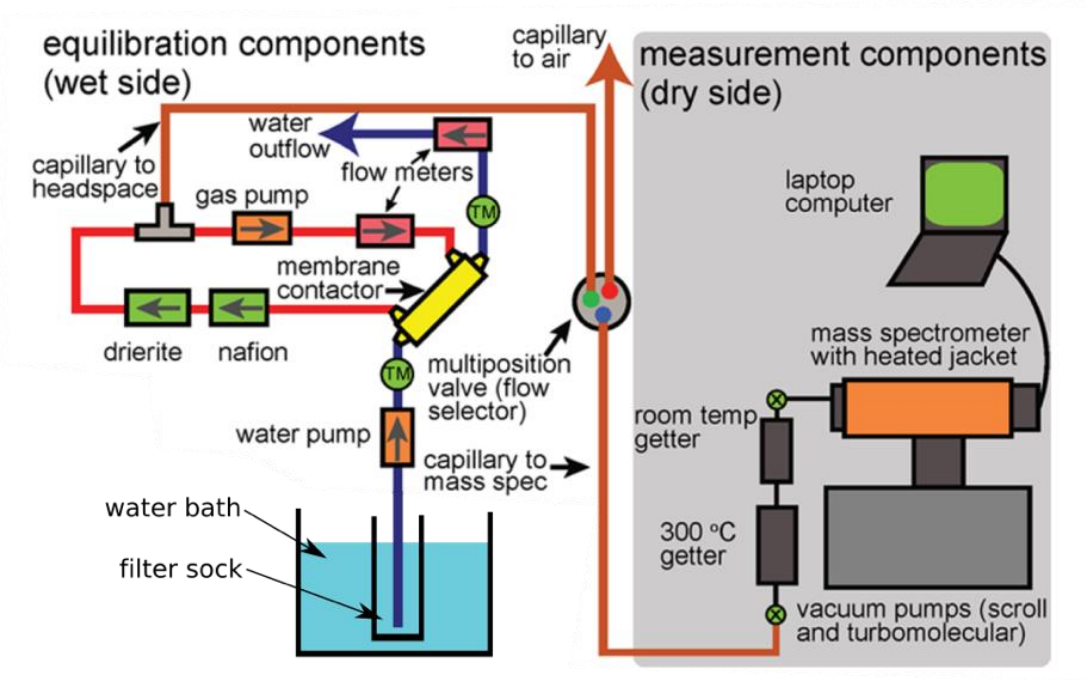

Figure 3: A schematic of the instrumental setup of the GEMS system. Adapted from Manning, et al. [35]

The system can be divided into equilibration components and measurement components. The equilibration side is mainly composed of a temperature-controlled water bath, a membrane contractor cartridge, and the drying components (Drierite and a Nafion box). During sample collection, water is filtered through a felt filter sock (2-layer, 5 mm inner, 100 mm outer pore size, 12'' long x 1.5'' wide), which is then pumped into the membrane contractor cartridge. The membrane contractor cartridge used in this system is a 3M Liqui-Cel Extra-Flow 2.5 × 8, model G540. The cartridge contains porous hollow fiber membranes, called lumens, made from a mixture of polypropylene and polyethylene. [35, 40] Water enters the cartridge and flows

outside of the lumens. Dissolved gases partition across the lumens into the headspace of the cartridge and the now degassed water flows out of the cartridge and back into the water bath. The Liqui-Cel Extra-Flow cartridge was chosen in particular because its design utilizes a central baffle to force liquids radially over the lumens, which promotes gas transfer compared to cartridge designs that flow water parallel to the lumens. Liquid water does not transfer across the membrane, but water vapor is able to transfer across the membrane where it condenses and clogs the pores. The clogged pores result in greater mass transport resistance and thus decreased gas transfer.[41]

In order to circumvent this issue, the gas is constantly circulated using an air pump and dried. The drying process is made up of two components. The equilibrated air is first circulated into a Perma-Pure Nafion desiccant box, which combines the selectivity of Nafion in absorbing water vapor with the dry purge environment created by molecular sieve desiccant. Air then flows into a 12'' long piece of Tygon tubing containing approximately 10 g of indicating Drierite (CaSO4, 10−20 mesh).

The operation of the GEMS is contingent on the equilibration of the air in the headspace with the flowing water.[35] By achieving equilibration, the noble gas ratios in water can be calculated from the measured noble gas ratios and Henry's Law. Using air-equilibrated water should result in ratios of the partial pressures of the noble gases in the headspace that are equal to those in air. In order to ensure that the equilibrium is established between the headspace and the water, capillary dimensions are chosen such that the flow rate out of the headspace is small compared to the rate of gas transfer across the membrane. Prior to modification, 5 m of 0.05 mm ID deactivated fused silica capillary was used to transfer gas from the headspace to the mass

spectrometer. A simplified version of the Hagen-Poiseuille fluid dynamic law was used to approximate the capillary flow rate:

$$Q_c \approx 10^3 \left(\frac{\pi r^4 P}{16 L \eta}\right) \quad (4)$$

where Q_c is the capillary flow rate, r and L are the radius and length of the capillary (m), P is the absolute pressure (Pa) of the headspace, and η is the gas dynamic viscosity (Pa-s).[42] The absolute pressure of the headspace was assumed to be about 1 atm (approximately 10^5 Pa). The gas dynamic viscosity of standard air at 300 K was used in calculations, which is equal to 1.87 x 10^5 Pa-s. Using this equation, the capillary flow rate with the fused silica capillary was calculated to be approximately 8.31 x 10^{-8} L/s.

Capillary of the same dimensions is used to sample ambient air periodically as a calibration standard. Since they are well-known and constant, noble gas mole ratios in ambient air can be used to convert the measured gas ratios to a saturation anomaly. The switch between ambient air and headspace air is performed using a VICI Valco multiposition valve. One meter of fused silica capillary is connected between the gas recirculation loop and the multiposition valve, one meter of fused silica capillary is connected to the multiposition valve with the other side open to ambient air, and 4 meters of fused silica capillary are connected between the constantly open central position of the multiposition valve and the mass spectrometer. The switches are performed automatically using a custom Visual Basic program that logs and controls changes in the positions of the multiposition valve. Additionally, the Visual Basic program records the flow rate using flowmeters and temperature from the thermistors, denoted with green circles in Figure 3, to account for temperature effects on the saturation state of the noble gases.

After flowing out of the multiposition valve, air is purified through a series of two custom-made getter chambers. Both chambers contain SAES Getters St2002 pellets to remove reactive and abundant gases such as H_2, N_2, H_2O, CH_4, and CO_2. The first getter chamber is heated to 300°C to adsorb all gases except for H_2 and the noble gases and to break the C-H bonds in CH_4. The second getter adsorbs H_2 from decomposed CH_4 and atmospheric H_2 gas. The getters are activated by heating them to 400°C for one hour. Reactivation of the getters is required when the signal intensity of N_2 (m/z =28) is comparable to that of ^{40}Ar.

Gases are then analyzed in a Hiden Analytical HAL 3F RC 201 quadrupole mass spectrometer. The mass spectrometer system is evacuated with a TPS-Compact with Turbo-V 301 Navigator turbomolecular and IDP-3 dry scroll pump. The HAL 3F RC 201 utilizes an electron impact ionizer with an Iridium filament and contains both a Faraday cup and a secondary electron multiplier (SEM) detector. It has a limit of detection of 5×10^{-4} mbar, making it suitable for measuring the low concentrations of noble gases in water. The Hiden mass spectrometer is used in particular (as opposed to quadrupole mass spectrometers of other brands) because of its ability to scan through a series of different mass to charge ratios at different electron energies in a repeated sequence. By doing so, the scanning parameters can be optimized for each of the noble gases, which can differ in signal by several orders of magnitude, and in particular, can be used to measure mass 22, Ne, without interference from doubly-charged mass 44, CO.

2.2 Mass Spectrometer Parameters

Our system is used to analyze isotopes of Ne, Ar, Kr, and Xe. Measurements of He were tested on the most abundant isotope of ^4He. Neon is measured on ^{22}Ne instead of ^{20}Ne, the most abundant isotope, because of interference by singly charged H_2O which also has a mass-to-charge ratio (m/z) of 20 and because of interference of doubly charged ^{40}Ar. Argon is analyzed

using ^{36}Ar, which has an abundance of 0.337% in the atmosphere, and ^{38}Ar, which has an abundance of 0.0629%. [35] Although it is the most abundant isotope of Argon, ^{40}Ar is not analyzed because the signal intensity is too large and cannot be measured accurately on the SEM detector without harming the detector. [43] Argon-38 is typically preferred because it can be measured on the same amplifier as ^{84}Kr. However, ^{36}Ar produces a larger signal so both isotopes of Ar were measured initially. Kr is analyzed with the most abundant isotope of ^{84}Kr, which has 57.0% abundance. Xe is analyzed with ^{129}Xe, which has an abundance of 26.4%. All noble gases are assumed to be singly-charged to give mass to charge ratios (m/z) equal to the mass of the atoms.

The mass spectrometer scans are performed in multiple ion detection (MID) mode in which all of the noble gases are measured in sequential order at their respective optimal parameters. The ion source parameters are summarized in Table 1, and the typical scan parameters are summarized in Table 2. Prior to January 8, 2018, background scans were done manually for each noble gas by measuring a mass-to-charge ratio that should not produce any signal. The background masses are denoted in Table 2 in the rows denoted with a (b). ^{22}Ne is measured at a reduced electron energy and emission in order to avoid production of doubly charged CO_2, which also has a mass-to-charge ratio of 22. By restricting the electron energy to below 37 V, production of doubly charged CO_2 can be reduced at the cost of decreasing the signal intensity. The emission has to be reduced along with the electron energy to avoid overloading the filament. The dwell time describes the amount of the time that a measurement is performed on a single mass and the settle time describes the amount of time that the system waits before the next measurement. The settle time is larger between measurements where the electron energy changes in order to allow the system to stabilize.

Table 1: Ion Source Settings

Multiplier	1500 V
Focus	-90 V
Cage	5.5 V
Electron-energy	70 or 35 V
Emission	1000 or 500 μA
Mode-charge	1000 ms

Table 2: Acquisition Settings for MID Experiments Prior to January 8, 2018 where (b) denotes the background masses

Gas	Mass (m/z)	Acquisition range (torr)	Dwell time(ms)	Settle time(ms)	Electron energy (V)	Emission current (μA)
^{4}He	4	10^{-9}	6000	500	70	1000
^{4}He(b)	5.5	10^{-9}	1000	4000	70	1000
^{22}Ne(b)	10.5	10^{-11}	1000	4000	35	500
^{22}Ne	22	10^{-11}	6000	500	35	500
^{38}Ar (b)	25.5	10^{-10}	1000	4000	35	500
^{38}Ar	38	10^{-10}	6000	1000	35	500
^{36}Ar(b)	24.5	10^{-8}	1000	500	70	1000
^{36}Ar	36	10^{-8}	2000	500	70	1000
^{84}Kr(b)	75.5	10^{-10}	1000	500	70	1000

^{84}Kr	84	10^{-10}	1000	500	70	1000
^{129}Xe(b)	121.5	10^{-11}	1000	500	70	1000
^{129}Xe	129	10^{-11}	8000	500	70	1000

*(b)=background

A leak test was performed with the original system by spraying He gas at various points of the wet side and monitoring for signal increases with the mass spectrometer. Experiments with the fused silica capillary were then conducted with the parameters described in Table 2 and were done as a standard of comparison prior to attempts to leak-proof the system. In this project, we refer to the type of experiments we conduct as air-water switching experiments. Air-water switching experiments involve switching between air equilibrated from water and air from the ambient atmosphere in one-hour intervals. These experiments may also be done with longer intervals, but we use one-hour intervals because it allows us to calibrate with air frequently and obtain a larger number of switches within an overall reasonable experiment length.

In all of the MID scans for the air-water switching experiments, a larger spike in signal intensity was observed at the beginning of each scan, which soon decreased after 2-3 cycles and stabilized. Although this problem did not appear to affect the measurements beyond the first couple cycles, experiments were conducted to determine the cause of the issue. Concurrently, scans were done on an older template called 20170609HighSEMandXehighEmission.exp in order to determine whether the 10^{-9} amplifier was still as unstable as it was during experiments the previous summer. Scans performed on the older template showed stable measurements on the 10^{-9} amplifier and lacked the large signal at the beginning of the scan that the newer scan had. A scan on the older template was performed again to determine if the steady signal was reproducible, but the filament burnt out while the scan was running.

The filament was replaced and an ion source tuning was attempted to optimize the ion source settings to give the highest quality signal, which remained the original settings as listed in Table 1. However, after measuring Ne, all of the masses decreased in signal by an order of magnitude. In some scans, the signal for all of the masses dropped off completely after a couple of cycles. A series of experiments were initiated in order to isolate the problem causing the signal decrease. Experiments varied conditions such as whether the scan was started in a new window or whether it was started in an existing window. The electron energy and the emission were also varied to determine whether the signal decreased between changes in ion source settings. After conducting these experiments, we concluded that the signal drop occurred when the scan was started in a new window with a change in electron energy.

However, consultation with Hiden suggested that starting a scan in a new window was indistinguishable from starting a scan in an existing window. Representatives from Hiden proposed that a contamination may be the source of the problems with signal. A bar scan on the Faraday cup was run on an emission of 2000 V overnight in order to attempt to burn out any contaminant. However, the signal drop was still being observed after this attempt. A charging test was then done to determine if there was a contaminant and the test indicated that there was no contaminant in the quadrupole filter of the mass spectrometer. The filament was changed again to ensure that the problem did not arise from the process of changing the filament or the filament itself. A series of scans varying the electron energy and whether the scan was started in a new window was done and continued to show a signal drop after changing the electron energy and starting a scan in a new window.

Because efforts to troubleshoot the signal drop were inconclusive, we decided to continue experimentation using He, Ar, and Kr because they are the most abundant of the suite of noble

gases and thus, still had a detectable signal despite the signal drop. In addition, Ne was not measured in order to avoid the additional signal drop that appeared to be caused by changing the electron energy. The acquisition settings for the MID experiments were changed in response to the new signal ranges. In addition, subsequent scans used auto-zero and auto-range, which automatically subtract the background and change the amplifier in response to signal changes, respectively. The settings for experiments performed after January 9, 2018 are summarized in Table 3.

Table 3: Acquisition Settings for MID Experiments After January 9, 2018

Gas	Mass (m/z)	Acquisition range (torr)	Dwell time(ms)	Settle time(ms)	Electron energy (V)	Emission current (μA)
^{4}He(b)	5.5	10^{-10}	1000	500	70	1000
^{4}He	4	10^{-10}	8000	500	70	1000
^{36}Ar(b)	24.5	10^{-8}	1000	500	70	1000
^{36}Ar	36	10^{-8}	4000	500	70	1000
^{84}Kr(b)	75.5	10^{-9}	1000	500	70	1000
^{84}Kr	84	10^{-9}	8000	500	70	1000

*b=background

2.3. Adapting the System for Helium Measurements

The gas circulation tubing on the wet side of the equilibration system was converted from McMaster-Carr flexible Tygon tubing to McMaster-Carr Viton tubing because Viton tubing is much less permeable to gases than Tygon tubing. The capillaries to transport gases were converted from 0.05 mm ID deactivated fused silica capillary to VICI Valco 1/16"OD x .004"ID (1.5875 mm OD x .1016 mm ID) Type 316 stainless steel tubing. The stainless steel capillary chosen for this experiment had the smallest inner diameter out of the off-the-shelf stainless steel

capillary options available. However, the inner diameter of the stainless steel capillary was still approximately twice that of the fused silica capillary. Using equation 4, the length of stainless steel capillary needed to produce the original flow rate of 8.31×10^{-8} L/s was calculated to be 85.2 m. Due to constraints in cost, three coils of 60' (~18.3 m) of stainless steel capillary were installed between the inlet valve and the VICI valve, between the VICI valve and the gas recirculation loop, and from the VICI valve with the other side open to air. Thus, the total length of capillary travelled by the sample gases is 120' (~36.6 m) and the new flow rate was calculated to be approximately 1.93×10^{-7} L/s.

Figure 4: The "dry" side of the wet board showing the VICI valve with the stainless steel capillaries extending from it.

The higher flow rate with the stainless steel capillary posed a potential issue with gas equilibration because the gas equilibration system relies on the gas being taken out of the headspace being small relative to the rate of gas diffusion across the membrane contractor. Moreover, He, with its low solubility, is difficult to equilibrate. As a result, experiments focused on ensuring that He equilibrates in the system. Initial experiments were conducted with the water bath set to 22°C. Experiments were then conducted at a lower water temperature of 10°C because gases are more difficult to equilibrate at lower temperatures. Assessment over whether He was equilibrating was uncertain and thus, Ne was added to the sequence of scans again. Because Ne should be slightly easier to equilibrate than He, Ne can be used to determine if He is effectively equilibrating. For instance, if Ne were not equilibrating, it is not likely that He is equilibrating as well. Thus, the acquisition settings were updated, which are summarized in Table 4.

Table 4: Acquisition Settings for MID scans after January 26, 2018

Gas	Mass (m/z)	Acquisition range (torr)	Dwell time(ms)	Settle time(ms)	Electron energy (V)	Emission current (μA)
^{4}He(b)	5.5	10^{-10}	1000	500	70	1000
^{4}He	4	10^{-10}	8000	500	70	1000
^{22}Ne(b)	10.5	10^{-12}	1000	1000	35	4000
^{22}Ne	22	10^{-12}	6000	6000	35	500
^{36}Ar(b)	24.5	10^{-8}	1000	500	70	1000
^{36}Ar	36	10^{-8}	4000	500	70	1000
^{84}Kr(b)	75.5	10^{-9}	1000	500	70	1000

^{84}Kr	84	10^{-9}	8000	500	70	1000

Improvements to the equilibration of the gases were attempted by increasing the air flow rate in the gas recirculation loop. By increasing the air flow rate, turbulence across the surface of the membrane increases, which promotes gas exchange. Since the gas flow-meters were not operational throughout the experiment, the air flow rate was expressed in terms of the voltage applied to the air pump through the DC power supply. Initial experiments used a voltage of 3.1 V, experiments after 1/19/18 used a voltage of 3.7 V, and experiments after 2/20/18 used a voltage of 4.2 V.

Air-water switching experiments performed after installation of the stainless steel capillaries occasionally showed rapid pressure fluctuations either during the air intervals or during the water intervals. This was attributed to either a contamination in the capillary or uneven openings in the capillary resulting in turbulent air flow. The stainless steel capillary was flushed with nitrogen air in an attempt to remove the contamination, but the pressure fluctuations continued. The stainless steel capillary used for the air calibration standard was cut by 0.8 cm with the VICI Precision Sampling Tubing Cutter for Steel Tubing. Cutting the capillary was done to smooth out the opening of the capillary. Both ends of the capillary between the VICI valve and the wet side of the equilibration components were cut as well by a total of 4.4 cm. Experiments to assess equilibration were then performed again.

In total, 19 air-water switching experiments were performed not including helium leak tests and other experiments done to study pressure fluctuations and troubleshoot problems with the mass spectrometer. The air-water switching experiments are summarized in Table 5.

Table 5: Summary of air-water switching experiments

Date(s)	Parameter Changed	Number of Experiments
11/3/17-11/5/17	Fused silica capillary	2
1/15/18-1/18/18	Stainless steel capillary	4
1/19/18-1/20/18	Higher air flow rate	2
1/23/18-2/1/18	Changed water bath temperature from 22°C to 10°C	7
2/8/18-2/9/18	Overnight experiment	2
2/20/18-2/21/18	Higher air flow rate	2

2.4 Data Analysis

Data analysis was completed using a custom script in MATLAB. Files in .csv format can be exported by MASSoft 7, the software for the Hiden mass spectrometer. The custom VisualBasic program records and exports temperature files, which also include approximate flow rate and pressure readings, and air files, which list the start and end times of the air calibration intervals. The three types of files are imported into MATLAB using the script. For data prior to 1/9/18, a background correction is done by subtracting the ion currents from the background masses from the respective noble gas ion currents. The ratios of the noble gases are then calculated by taking the ratio of the ion currents of the noble gases. The running mean of each ratio is taken in order to reduce noise. The mean of each ratio over the duration of each air calibration interval is calculated and the mean from each air calibration interval is linearly interpolated. The standard deviation of the absolute value of the difference between the running mean of the ratios and the linear interpolation of the ratios during the calibration intervals is defined as the precision of the data. Thus, a low numerical value of precision is a good precision

value because it represents a small deviation between the data during the calibration intervals and the data during the water intervals.

The raw data, linear interpolation, running mean, and air calibration intervals are plotted in order to visually determine how stable the data is. The ratio of the running mean of the ratios over the interpolated data is calculated and plotted to evaluate the deviation of the ratios during the water intervals from the calibration standard. When the system is equilibrating, the ratio of the running mean to the interpolated data should be equal to 1 so a ratio greater than 1 indicates oversaturation while a ratio less than 1 indicates undersaturation. Additionally, a t-test was performed on the ratio of the running mean to the interpolated data for each noble gas ratio during each water interval to determine whether the mean of the ratio of the running mean to the interpolated data was statistically different from 1. Comparing the ratio between various experiments allows us to assess the effectiveness of the equilibration method.

Chapter 3: Results and Discussion

Air-water switching experiments were first conducted with the original configuration with the fused silica capillary as a standard of comparison for subsequent experiments. The raw data, running mean, linear interpolation, and air intervals for each noble gas ratio are plotted in Figure 4 with the precision values printed in the title of each ratio plot. The precision values for the ratios including He (mass 4) are worse than those of the other ratios. This may be due to the permeability of He through multiple parts of the system. Figure 6 suggests that He could be equilibrating because the average of the deviation between the running mean and interpolated data is above 1. This is corroborated by Table 6, which summarizes the average values of the ratio of the running mean of the raw data and the linear interpolation of the air pockets. Table 6 indicates that the ratios with He are oversaturated for the 11/3/18 and 11/5/18 experiments because the average ratio is greater than 1. However, because of the likeliness that He was permeating in and out through the system, the extent of equilibration shown in Figure 6 and Table 6 may not be reliable.

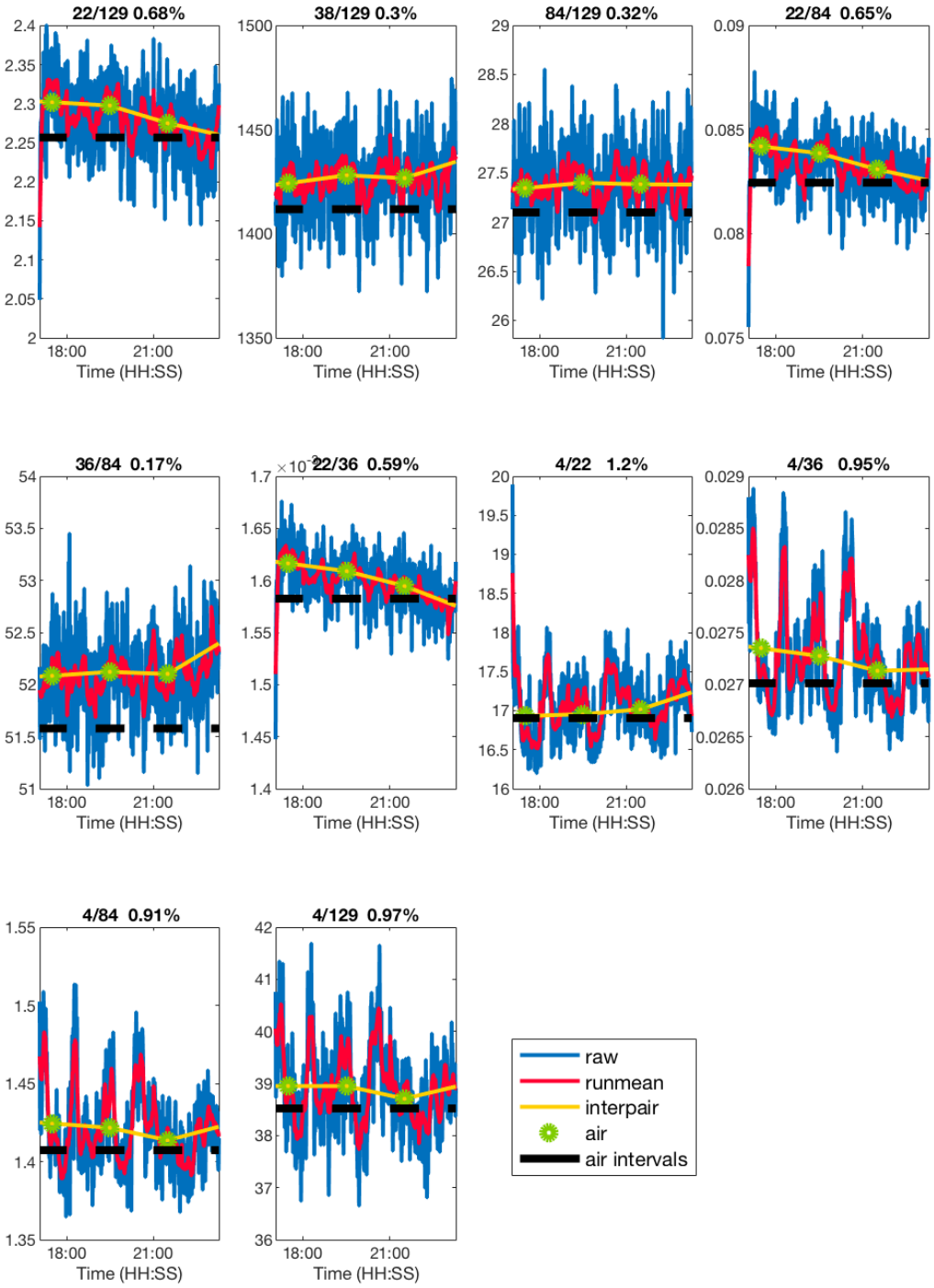

Figure 5: The noble gas ratios from the 11/5/17 air-water switching experiment with fused silica capillary and the water bath set to 22°C. The precision values are shown in the title of each ratio plot. The raw data is plotted in blue, the running mean of the raw data is plotted in red, the linear interpolation of the air pockets is plotted in yellow, and the black lines refer to the times at which the air calibration is being measured. The green circles are the mean of the data during the air intervals over which the linear interpolation is plotted.

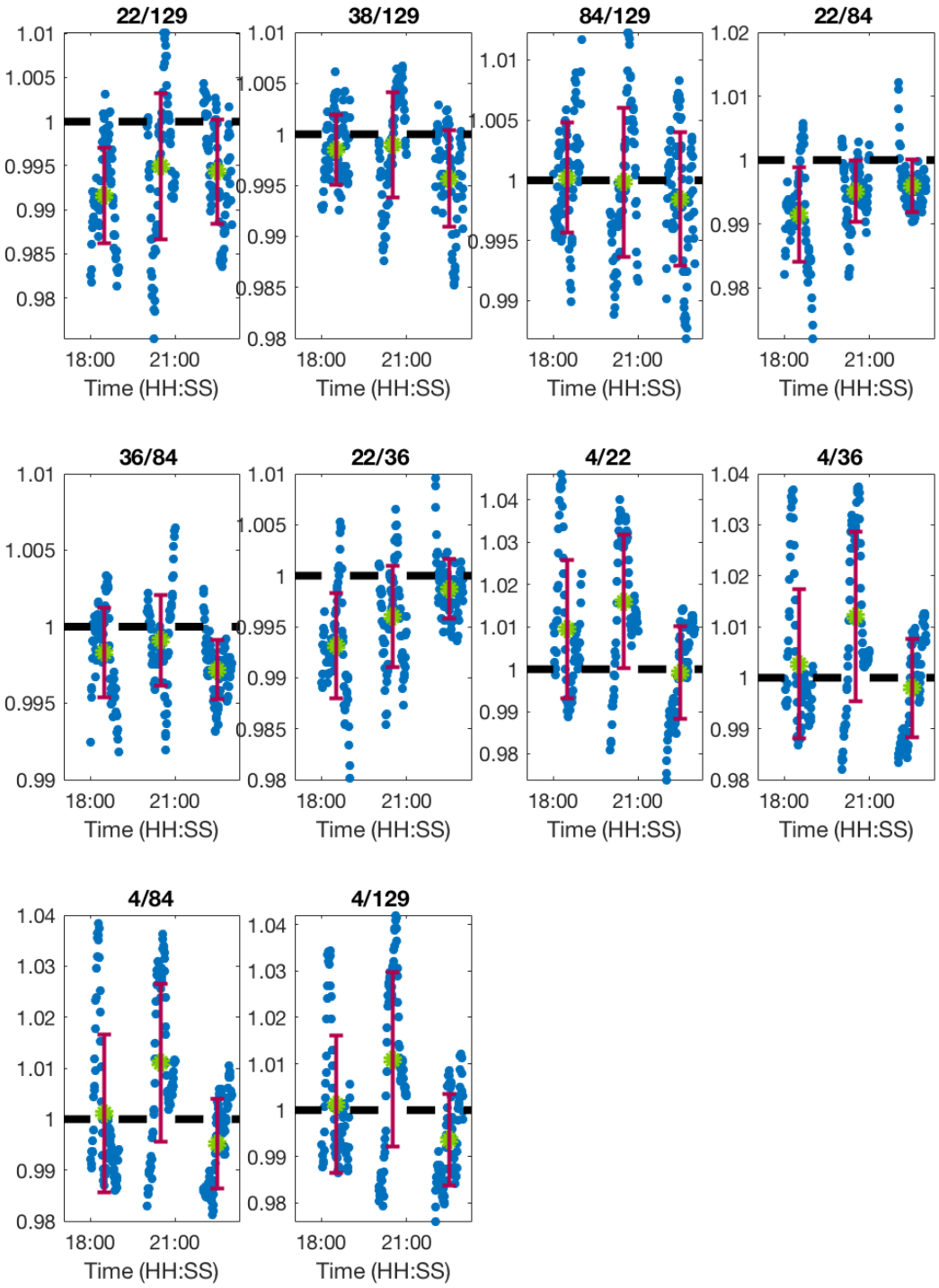

Figure 6: Ratio of the running mean and interpolated data from the 11/5/17 data during the air-water switching experiment with fused silica capillary and the water bath set to 22°C. This plot illustrates the difference between the air and water data. The ratios are plotted in blue, and the black lines refer to times at which the air calibration was measured and thus, the data was not plotted during those time intervals because they would equal 1. The green circles represent the mean of the ratios, and the red error bars illustrate the standard deviation from the mean.

Table 6: Average values of the ratio of the running mean and interpolated data for each water interval for all air-water switching experiments. The values highlighted in green are statistically different from 1.

Day	Water Pocket #	Ne/Xe	Ar/Xe	Kr/Xe	Ne/Kr	Ar/Kr	Ne/Ar	He/Ne	He/Ar	He/Kr	He/Xe
11/3/18	1	1.00	1.00	1.00	1.00	1.00	1.00	1.07	1.06	1.06	1.06
	2	1.00	1.00	1.00	1.00	1.00	1.00	1.02	1.01	1.01	1.01
	3	1.00	1.00	1.01	0.99	1.00	0.99	1.01	1.00	1.00	1.00
11/5/18	1	0.99	1.00	1.00	0.99	1.00	0.99	1.01	1.00	1.00	1.00
	2	0.99	1.00	1.00	1.00	1.00	1.00	1.02	1.01	1.01	1.01
	3	0.99	1.00	1.00	1.00	1.00	1.00	1.00	1.00	1.00	0.99
1/15/18	1					1.00			1.00	1.01	
	2					1.00			1.00	0.99	
1/16/18	1					1.00			1.00	1.00	
	2					1.00			0.99	1.00	
1/17/18	1					1.00			1.00	1.01	
	2					1.00			1.00	1.00	
	3					1.00			0.99	0.99	
1/18/18	1					1.00			1.00	1.00	
	2					1.00			1.00	1.00	
1/19/18	1					1.00			0.99	0.99	
	2					1.00			1.00	1.00	
	3					0.99			0.99	0.99	
1/20/18	1					1.00			1.01	1.00	
	2					0.99			1.00	0.99	
	3					1.00			1.00	1.00	
1/23/18	1					1.00			0.99	0.98	
	2					1.01			0.97	0.98	
	3					1.01			0.98	0.99	
1/24/18	1					1.01			0.99	1.00	
	2					1.01			0.98	0.99	
	3					1.01			0.97	0.97	
1/25/18	1					0.99			1.00	0.99	
	2					1.00			0.98	0.98	
	3					1.01			0.98	0.99	
1/26/18	1				0.82	0.98	0.84	1.20	1.01	0.99	
1/28/18	1				1.02	1.00	1.02	0.95	0.99	0.99	
1/31/18	1				0.95	1.00	0.95	1.02	0.97	0.97	
	2				0.99	1.00	0.99	1.00	0.99	0.99	
	3				1.02	0.99	1.02	0.96	0.99	0.99	
2/1/18	1				1.00	1.00	1.01	0.98	0.99	0.98	

	2	1.00	1.00	1.00	0.97	0.98	0.98
	3	1.00	1.01	1.00	0.99	0.99	0.99
2/8/18	1	0.99	0.99	1.00	0.99	0.99	0.98
	2	1.04	1.00	1.05	0.93	0.99	0.98
	3	0.99	1.00	1.00	0.99	0.99	0.98
	4	1.07	1.00	1.07	0.92	0.98	0.99
	5	0.96	0.99	0.97	1.04	1.01	1.00
	6	0.97	1.00	0.98	1.02	0.99	0.99
	7	1.02	1.00	1.02	0.96	0.98	0.98
	8	0.96	1.00	0.96	1.03	0.99	0.99
2/9/18	1	0.98	0.99	0.99	1.00	0.99	0.98
	2	1.02	1.00	1.02	0.97	0.99	0.99
	3	0.98	1.00	0.98	1.00	0.98	0.98
	4	0.98	0.99	0.99	1.00	0.99	0.98
	5	0.99	0.99	1.00	0.99	0.99	0.98
	6	1.03	1.00	1.03	0.96	0.99	0.98
	7	1.02	0.99	1.03	0.97	1.00	0.99
2/20/18	1	1.02	1.00	1.02	0.94	0.97	0.97
	2	1.03	1.01	1.02	0.97	0.98	0.99
	3	0.99	0.99	0.99	0.99	0.98	0.98
	4	1.02	1.00	1.02	0.97	0.99	0.99
	5	1.03	1.00	1.03	0.95	0.98	0.98
2/21/18	1	1.04	1.01	1.03	0.95	0.98	0.99
	2	0.97	0.99	0.98	1.01	0.99	0.98
	3	1.02	1.00	1.02	0.95	0.97	0.98
	4	1.01	1.00	1.02	0.97	0.99	0.99
	5	1.00	0.99	1.01	0.98	0.99	0.98
	6	0.98	0.99	0.99	0.99	0.98	0.97
	7	0.99	0.99	1.00	0.99	0.98	0.97

Table 7: T-test values of the ratio of the running mean and interpolated data for each water interval for all air-water switching experiments. The t-test values highlighted in green represent the data sets with mean values that are statistically different from 1.

Day	Water Pocket #	Ne/Xe	Ar/Xe	Kr/Xe	Ne/Kr	Ar/Kr	Ne/Ar	He/Ne	He/Ar	He/Kr	He/Xe
11/3/18	1	2.12	0.167	1.42	3.77	2.26	2.78	31.8	34.5	31.4	31.6
	2	2.44	0.466	0.938	3.76	1.00	3.56	13.4	14.9	12.2	11.1
	3	2.14	2.49	4.62	6.50	4.54	5.63	5.35	0.817	2.02	2.49
11/5/18	1	6.67	1.44	0.395	7.94	2.67	7.68	5.72	2.07	0.818	0.992
	2	3.56	1.07	0.189	4.47	2.20	3.96	10.8	9.20	8.26	7.05

	3	4.13	4.69	1.48	3.57	5.34	1.36	0.462	2.04	4.47	4.74
1/15/18	1					2.32			0.625	2.10	
	2					2.04			1.83	2.59	
1/16/18	1					3.21			3.64	0.871	
	2					0.806			3.95	2.87	
1/17/18	1					2.36			0.162	1.55	
	2					1.45			0.0989	0.776	
	3					0.446			3.91	3.49	
1/18/18	1					0.0595			0.302	0.262	
	2					1.89			0.117	1.56	
1/19/18	1					1.45			4.38	1.91	
	2					0.0151			0.368	0.461	
	3					4.72			2.15	4.14	
1/20/18	1					3.36			2.65	0.155	
	2					4.70			0.582	3.46	
	3					3.32			1.57	0.752	
1/23/18	1					1.77			6.55	5.86	
	2					3.69			12.6	8.54	
	3					4.71			9.45	5.56	
1/24/18	1					5.40			6.96	1.31	
	2					2.21			5.15	3.72	
	3					4.12			11.7	12.2	
1/25/18	1					2.70			2.63	3.96	
	2					3.29			11.4	8.19	
	3					3.29			8.82	4.70	
1/26/18	1				9.48	5.43	7.89	6.72	1.91	0.689	
1/28/18	1				1.02	1.09	1.37	3.28	1.06	1.99	
1/31/18	1				3.91	0.254	4.15	1.87	8.04	9.92	
	2				0.137	0.586	0.245	1.15	2.65	2.69	
	3				2.51	3.59	3.12	5.55	2.73	3.78	
2/1/18	1				0.892	3.46	1.76	3.63	4.22	5.40	

	2	0.0792	0.690	0.0809	2.63	6.31	5.42
	3	0.577	1.00	0.872	0.856	3.75	2.99
2/8/18	1	1.09	11.4	1.19	3.19	3.85	8.76
	2	7.82	3.17	8.36	12.1	6.68	7.91
	3	0.427	4.72	1.38	4.01	5.92	9.07
	4	13.8	2.94	13.4	16.7	7.39	5.01
	5	5.66	7.39	4.51	4.77	0.0679	3.39
	6	5.79	1.19	4.80	3.35	3.80	4.08
	7	4.46	0.801	4.28	6.60	7.71	5.40
	8	8.14	5.54	6.41	3.85	4.70	6.52
2/9/18	1	2.72	6.15	1.74	0.605	4.69	8.55
	2	3.72	0.648	3.86	5.11	4.84	5.01
	3	1.93	0.870	1.60	3.03	10.7	10.2
	4	2.41	8.84	0.00459	2.07	5.89	9.85
	5	0.859	8.16	0.895	2.22	4.35	8.57
	6	5.37	0.986	5.37	7.61	5.11	5.32
	7	3.14	10.2	4.84	3.87	0.613	6.58
2/20/18	1	2.23	1.43	2.50	6.76	12.2	9.91
	2	4.20	5.55	3.29	4.53	5.42	2.52
	3	1.28	3.02	0.972	0.303	6.94	8.18
	4	3.29	0.305	3.54	4.81	4.10	3.42
	5	4.75	1.45	5.25	7.83	6.67	6.66
2/21/18	1	5.98	6.78	4.84	6.87	7.26	3.46
	2	6.05	7.89	4.85	1.80	5.92	9.12
	3	2.52	1.22	2.17	8.74	16.1	13.3
	4	1.46	2.86	2.17	3.73	6.34	6.36
	5	2.79	8.60	0.576	1.30	2.13	5.74
	6	5.31	3.96	4.29	0.874	12.4	12.2
	7	0.790	7.25	0.0474	1.35	10.1	12.7

A preliminary He leak test was performed over the original configuration of the system to approximate areas where He leakage was most significant. The He leak test showed a significant

increase on the order of 10^{-8} torr when He was sprayed over the gas recirculation tubing and the capillary going into the inlet valve of the mass spectrometer system. These tests reaffirmed the need to switch the gas recirculation tubing from Tygon to Viton tubing and the capillary from fused silica to stainless steel.

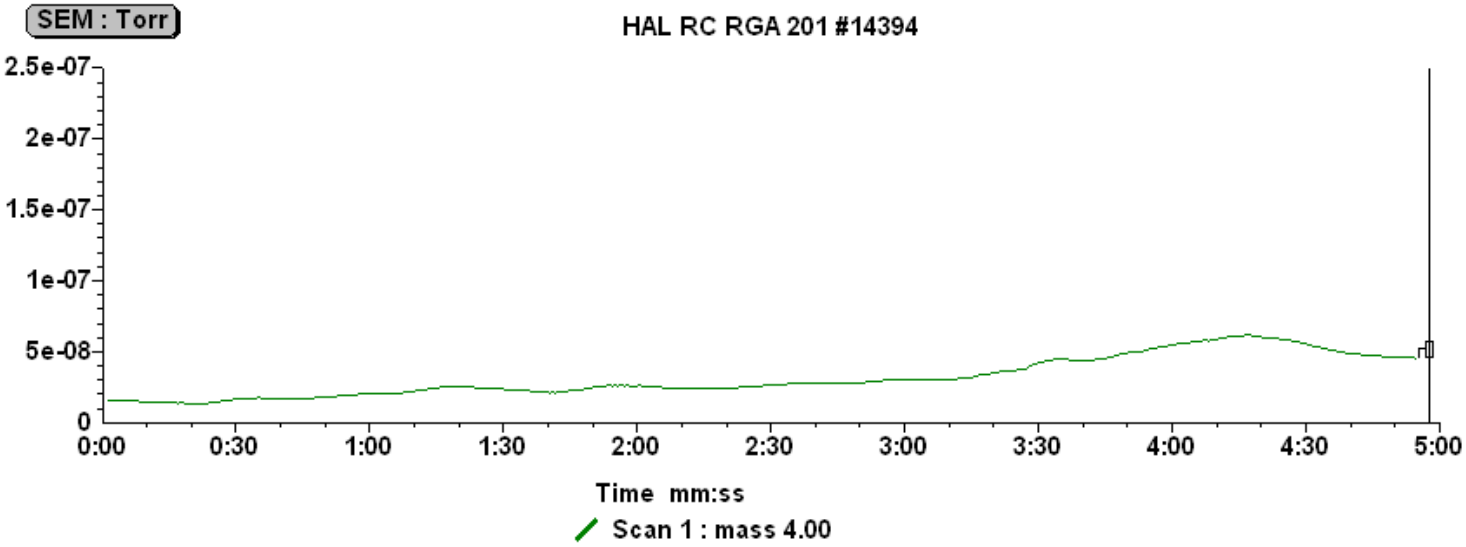

Figure 7: Helium leak test of the original configuration of the system.

Table 8: Parts of the system assessed with the He leak test of the original configuration

Part of the System	Time Corresponding to Fig. 6 (mm:ss)
Equilibrator Cartridge: Gas in Port	0:18-0:35
Equilibrator Cartridge: Water out Port	0:35-1:05
Equilibrator Cartridge: Gas out Port	1:05-1:40
Equilibrator Cartridge: Water in Port	1:40-2:05
Equilibrator Cartridge: Insulation Foam	2:05-2:40
Equilibrator Cartridge: Plastic surface	2:40-3:20
Gas tubing	3:20-4:00
Fused Silica Capillary (near inlet valve)	4:00-end

A He leak test was performed on the new configuration of the system to determine whether the addition of the Viton tubing and stainless steel capillary improved the leak-tightness of the system. Figure 8 and Table 9 summarize the results of the He leak test. A significant increase in signal occurs around 7:30, but at that time, no part of the system was being sprayed with helium. It is likely that the sharp increase in signal around 7:30 is due to increasing He in the room rather than a leak through a part of the system. Additionally, the increase in signal is on the order of 10^{-10} torr whereas leaks in the system in the previous He test were on the order of 10^{-8}. Considering the signal drop of an order of magnitude inherent to the problems with the mass spectrometer, the increase in signal in the most recent He test is still small compared to the signal increase in the previous He test. Thus, it was concluded that no significant leaks of the system were present. An additional test to ensure the leak-tightness of the system could have been to cover the wet side of the system with a bag and filling it with He to determine the extent of He leakage into the system and definitively assess the impact on the signal if He were to fill the room. An effective application of this test would involve careful consideration of the material of the bag to ensure that He does not leak out of the bag.

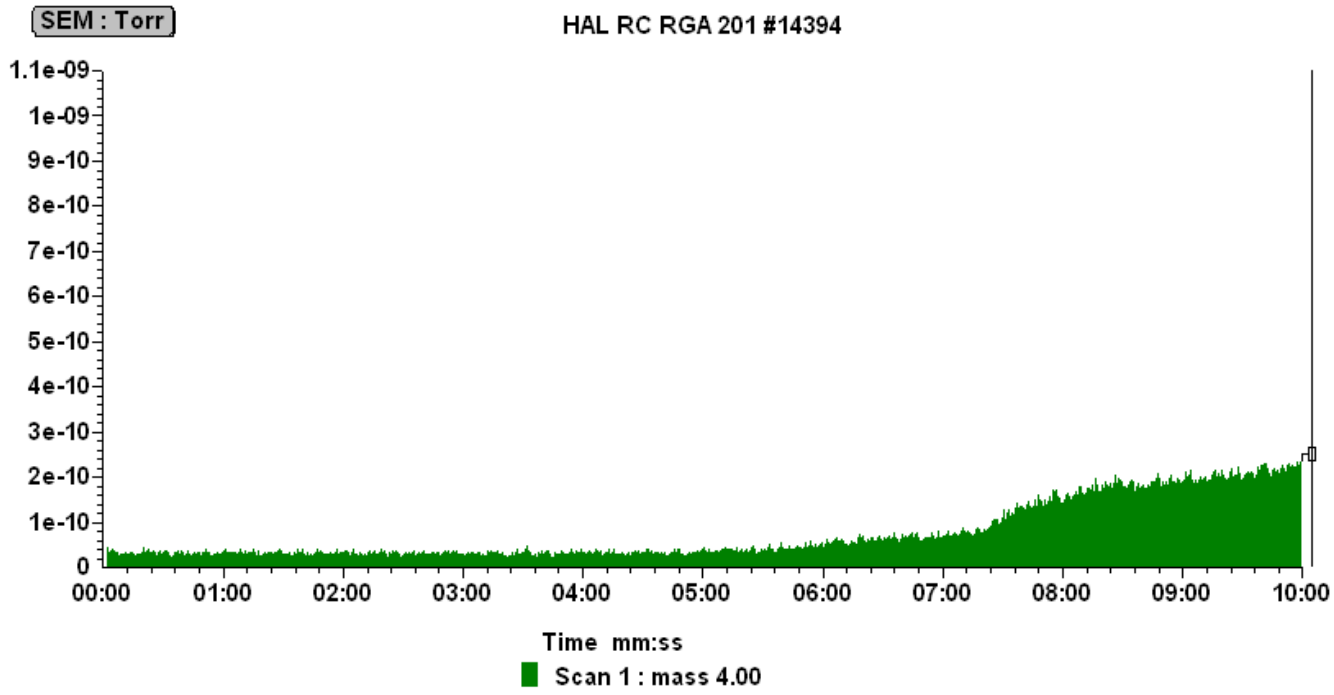

Figure 8: Helium leak test of the new configuration of the system with Viton tubing and stainless steel capillary.

Table 9: Parts of the System Assessed with the He leak test of the new configuration

Part of the System	Time Corresponding to Fig. 7 (mm:ss)
Equilibrator Cartridge: Water Out Port	0:55-1:25
Equilibrator Cartridge: Gas In Port	1:25-2:10
Equilibrator Cartridge: Water In Port	2:10:2:30
Equilibrator Cartridge: Gas Out Port	2:30-3:00
Nafion Box	3:00-4:07
Viton tubing on right side of wet board	4:07-4:48
T-Fitting	4:48-6:40
Break to open He tank further	6:40-7:43
Viton tubing on the left side of wet board	7:43-8:05
VICI port 6	8:05-8:25

VICI center port	8:25-8:42
Stainless Steel Capillary (near inlet valve)	8:42-end

Due to difficulties with the Hiden mass spectrometer as discussed in the previous chapter, the ion currents for all of the noble gases were an order of magnitude lower than the experiments performed in November. Thus, the experiments performed on the new configuration initially only include ratios of the most abundant gases: He, Ar, and Kr.

The first experiments with the new configuration were performed with the water bath set to 22°C. We were initially concerned that the larger diameter of the stainless steel capillary compared to the fused silica capillary would significantly increase the pressure inside the mass spectrometer. A significant increase in pressure would be harmful to the SEM detector in the mass spectrometer. However, the pressure only rose to 1.7×10^{-7} torr from 1.1×10^{-7} torr with the fused silica capillary despite the expected doubled air flow rate through the capillary. The experiments with the new configuration showed improved precision for the ratios with He and consistent ratios between measuring in air versus water. This suggests that the system is equilibrating since the sampled water is equilibrated with air so if the equilibration system is working properly, we would expect the ratios in water to be the same as in air. Figure 10 and Table 6 reaffirm this finding since the deviation of the running mean from the interpolated data is on average approximately 1, suggesting that the system is equilibrating. Further experiments (Figures 11 and 12) were conducted to improve the equilibration by increasing the air flow rate. The findings from these experiments did not show significant improvement of the equilibration with an increase in flow rate.

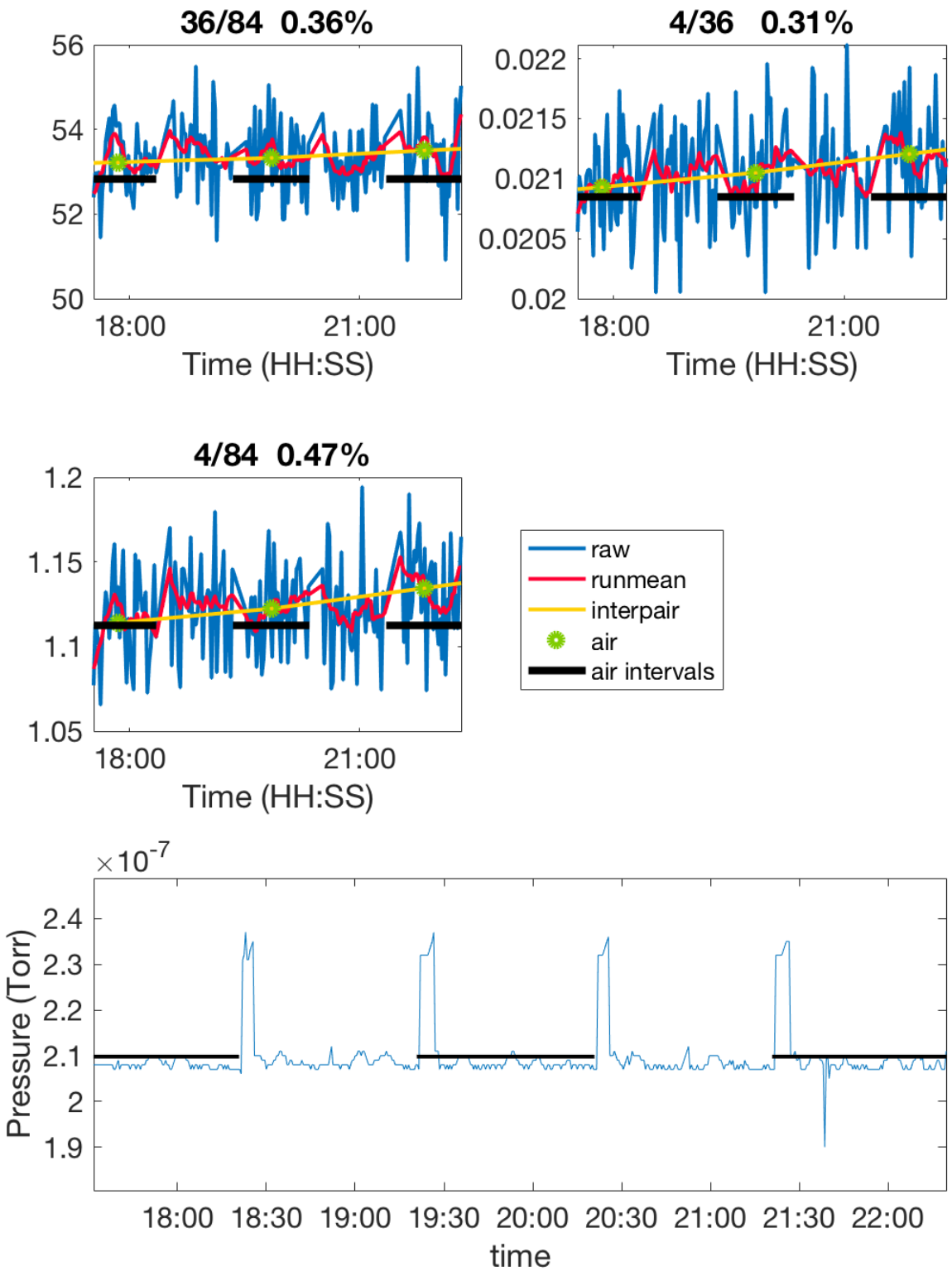

Figure 9: The top 3 plots show the noble gas ratios from the 1/15/18 air-water switching experiment with stainless steel capillary with the water bath set to 22°C. Data are plotted in the same way as in Fig. 5. The bottom plot shows the pressure over time.

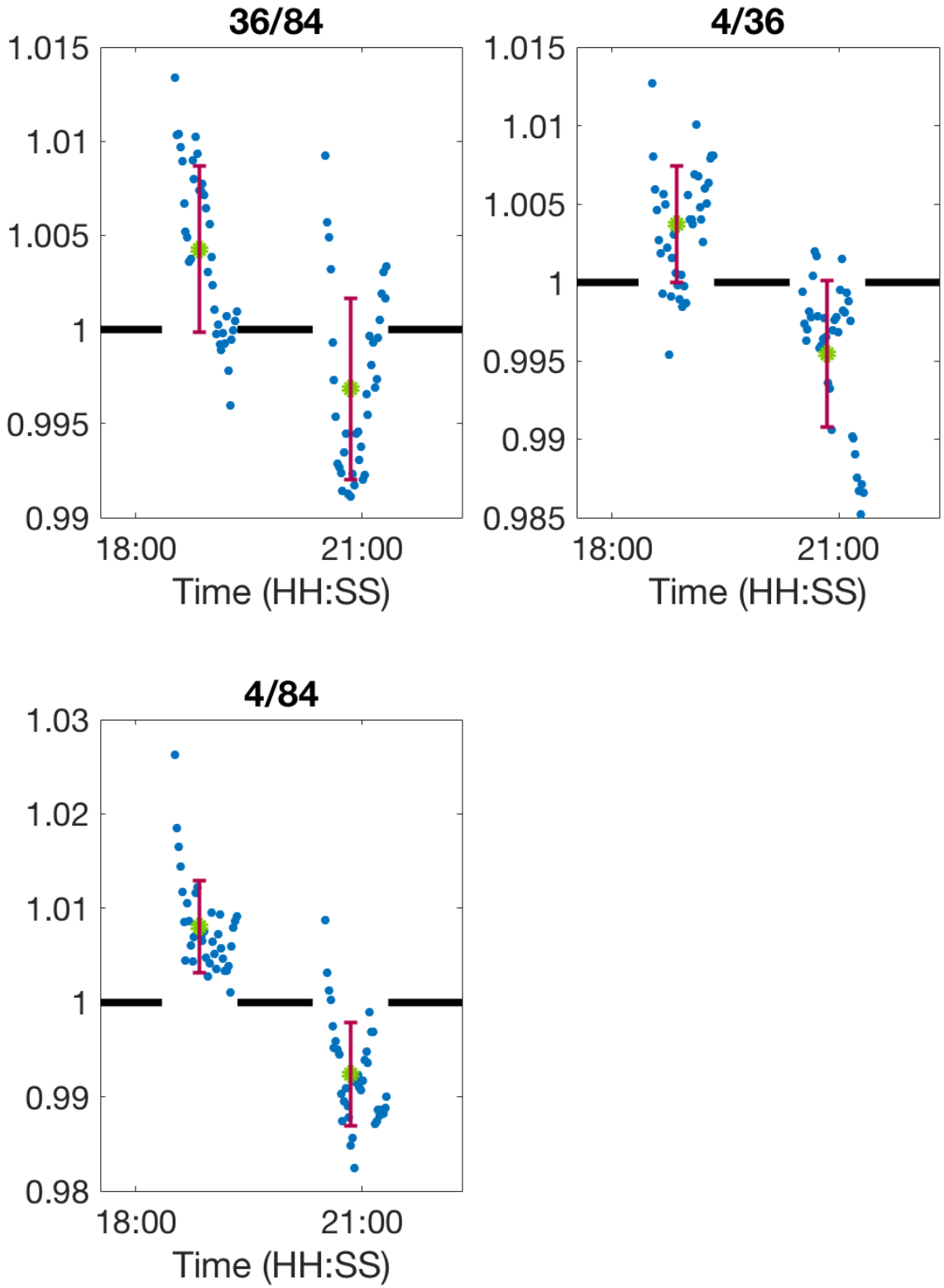

Figure 10: Ratio of the running mean and interpolated data from the 1/15/18 data during the air-water switching experiment with stainless steel capillary and the water bath temperature set to 22°C. Data are plotted in the same way as in Fig. 6.

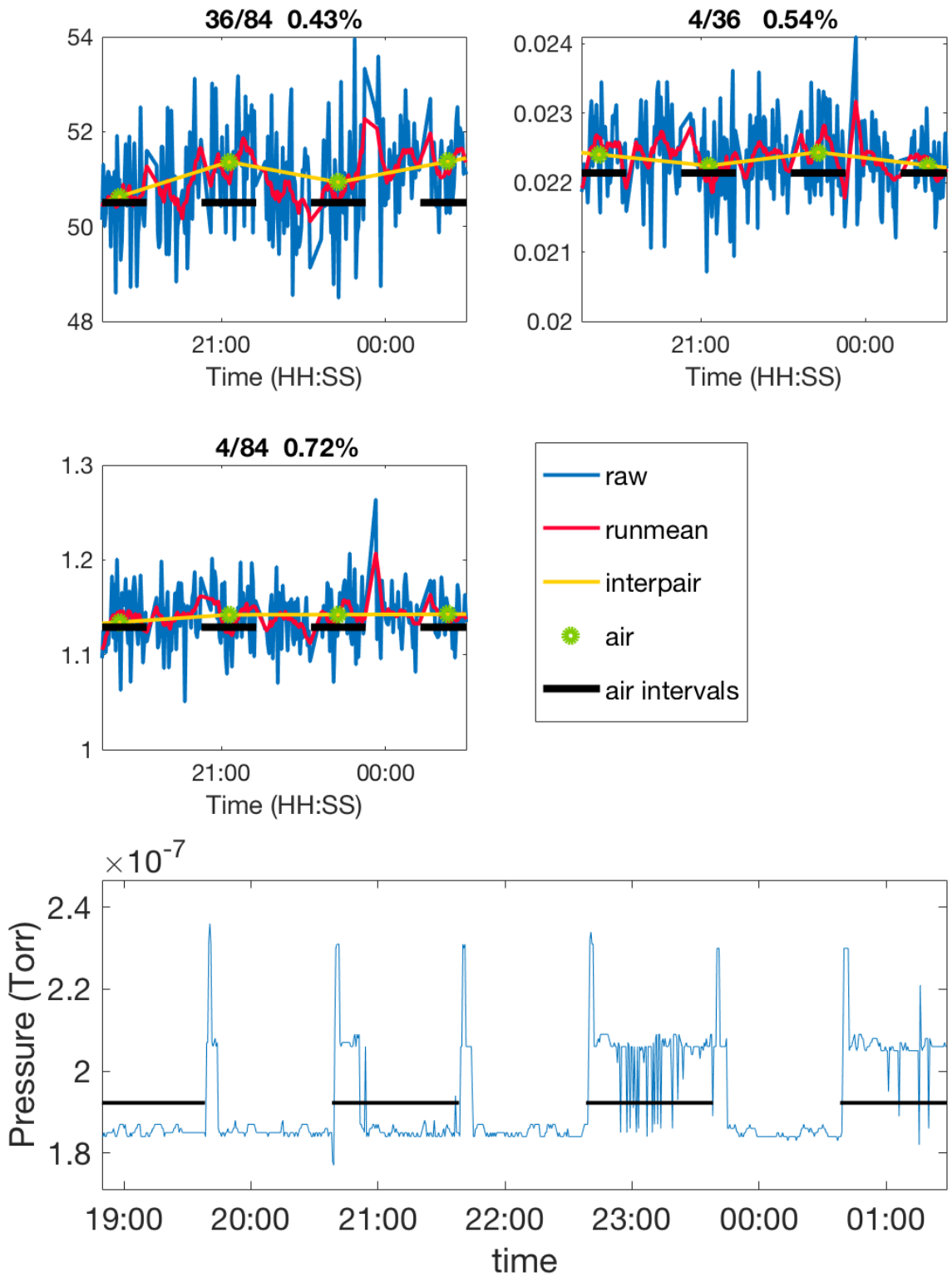

Figure 11: Noble gas ratios for the 1/20/18 air-water switching experiment with 22°C water and a higher air flow rate with a plot of pressure vs. time. Data are plotted in the same way as Fig. 9.

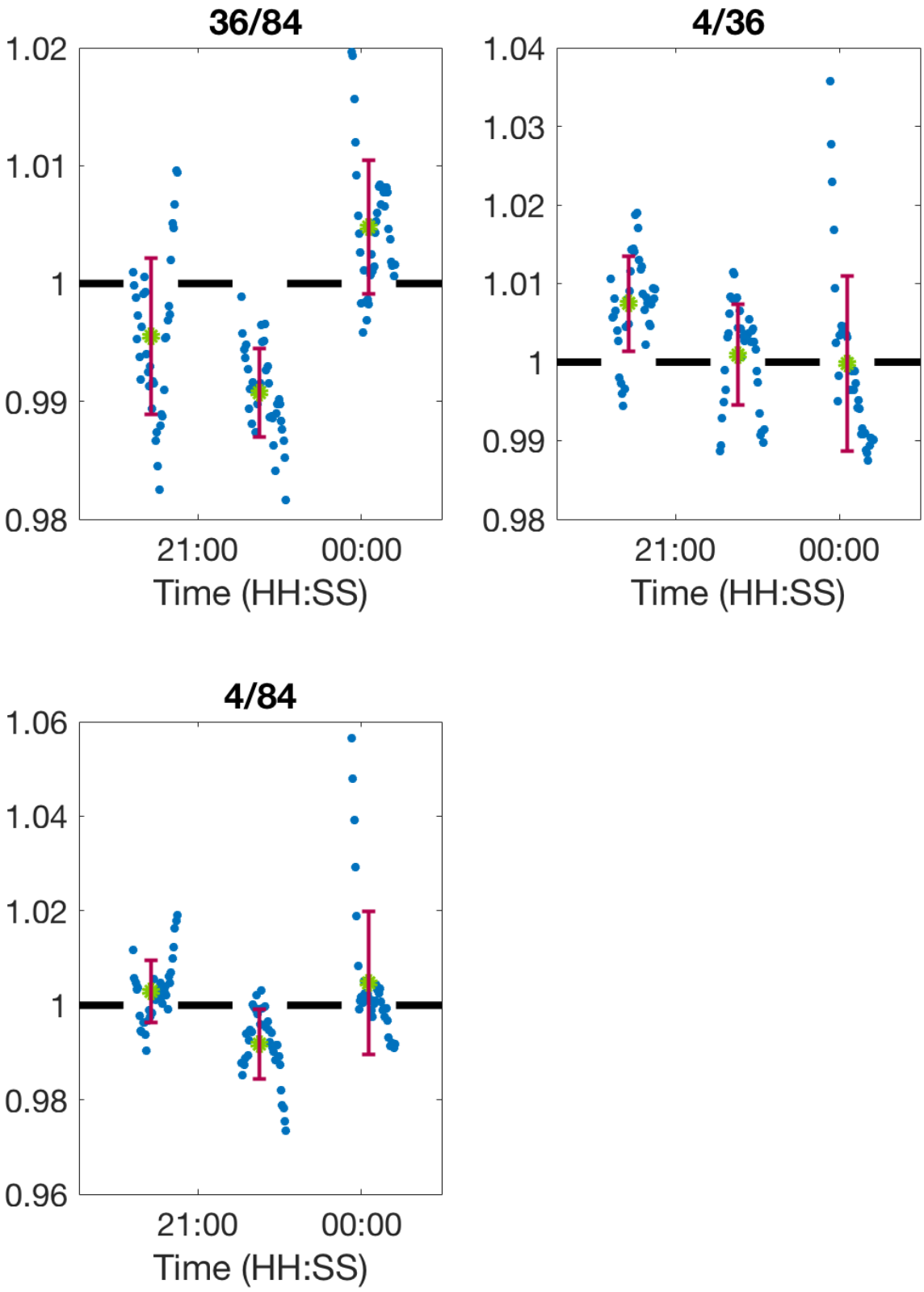

Figure 12: Ratio of the running mean and the interpolated data from the 1/20/18 data during the air-water switching experiment performed with stainless steel capillary in 22°C water with a higher air flow rate. Data are plotted the same way as in Fig. 6.

Unlike the experiments with fused silica capillary, experiments with the stainless steel capillary consistently showed a pressure spike of approximately 2×10^{-8} torr when switching between air and water before stabilizing. The pressure spike did not appear to affect the noble gas ratios since the ion currents for each noble gas increased by the same fraction. However, we were concerned that the pressure spike could indicate a leak in the system since it was not observed in experiments with the fused silica capillary. To investigate, the length of the air intervals was increased from 1 hour to 2 hours and 3 hours. If a leak existed in the system, the pressure spike should increase approximately linearly with respect to the length of the air interval. Instead, we observed that the pressure spike was consistently about 2×10^{-8} torr irrespective of the length of the air interval, indicating that the spike was due to air filling up the length of the stainless steel capillary and not due to a leak.

Initially, the pressure spikes in the ion current of all of the masses were conserved because they did not have a significant effect on the ratios. However, the calculation of the running mean was modified. Previously, the running mean was calculated for the entire experiment duration rather than for each air and water interval. Because the running mean was calculated this way, the running mean of the beginning and end of each air or water interval included data points from the preceding air or water interval. The calculation of the running mean was thus modified such that the running mean was calculated within each air and water interval and then concatenated to produce the running mean for the entire measurement duration. However, in doing so, the running mean reflected the pressure spikes in the raw data more sharply, which significantly affected the ratio of the running mean and interpolated data. Thus, the pressure spikes were excised from the data by removing the first ten minutes of data from the start of each air and water interval.

Because equilibration of the system appeared sufficient using water at 22°C, subsequent experiments were done with water at 10°C because equilibration is more difficult at lower temperatures and consideration of a range of water temperatures is necessary to assess the effectiveness of the system in the field. Figure 14 visually shows that the equilibration with the water at 10°C is worse than at 22°C. The average values in Table 6 support this finding and show undersaturation for the He ratios by 2-3%. Because water is more difficult to equilibrate at colder temperatures due to the lower diffusivity of the gases in cold water, it was possible that the equilibration worsened because the water in the water bath itself was not yet equilibrated or that gases were more slowly equilibrating out of the membrane cartridge. To ensure that the water in the water bath was equilibrated, the water was continuously circulated in and out of the wet side of the board to promote sufficient mixing of the water in the water bath prior to experiments. The water bath remained at 10°C for three days prior to the start of experimentation.

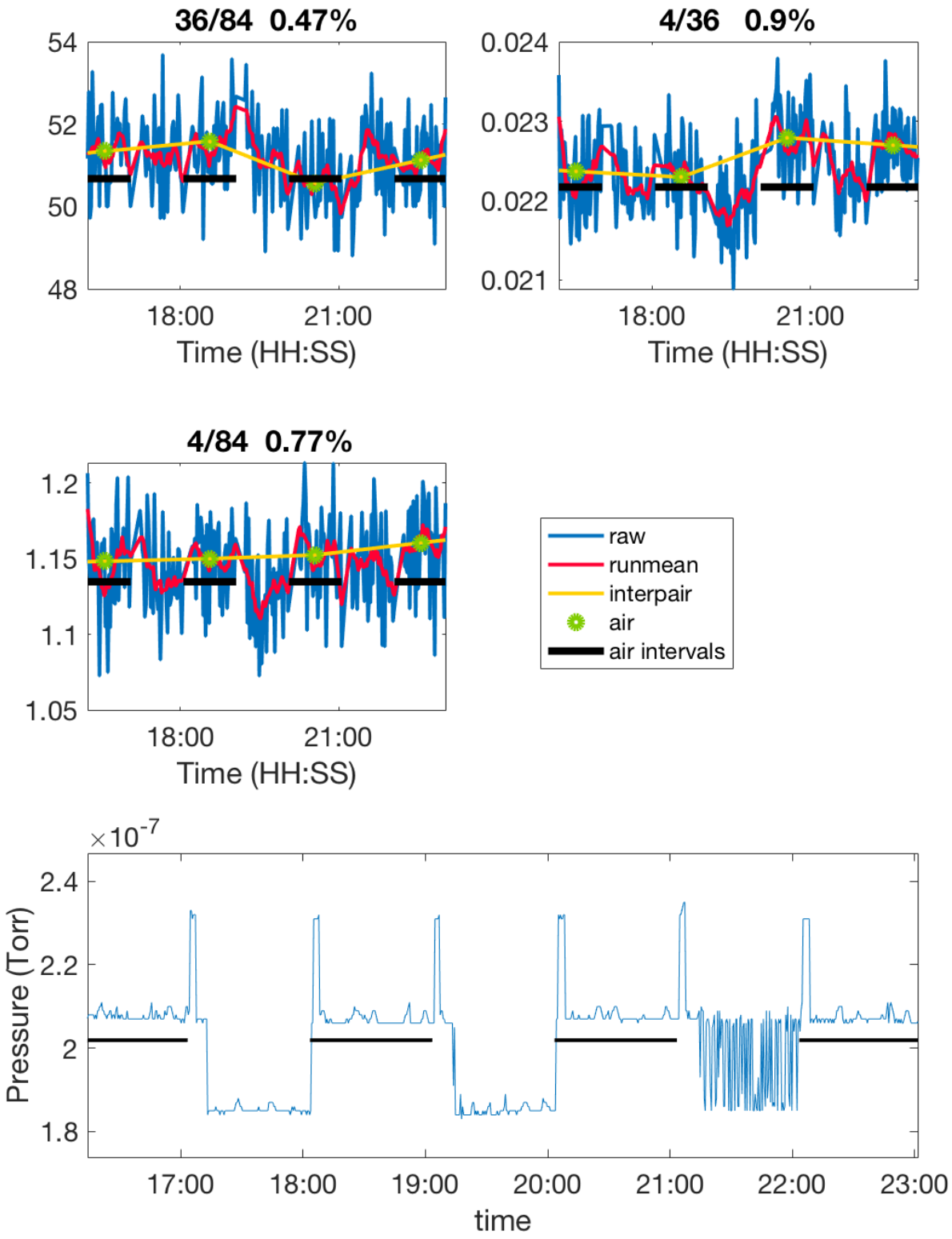

Figure 13: Noble gas ratios for the 1/25/18 air-water switching experiment with stainless steel capillary in 10°C water and a plot of pressure vs. time. Data are plotted in the same way as Fig. 9.

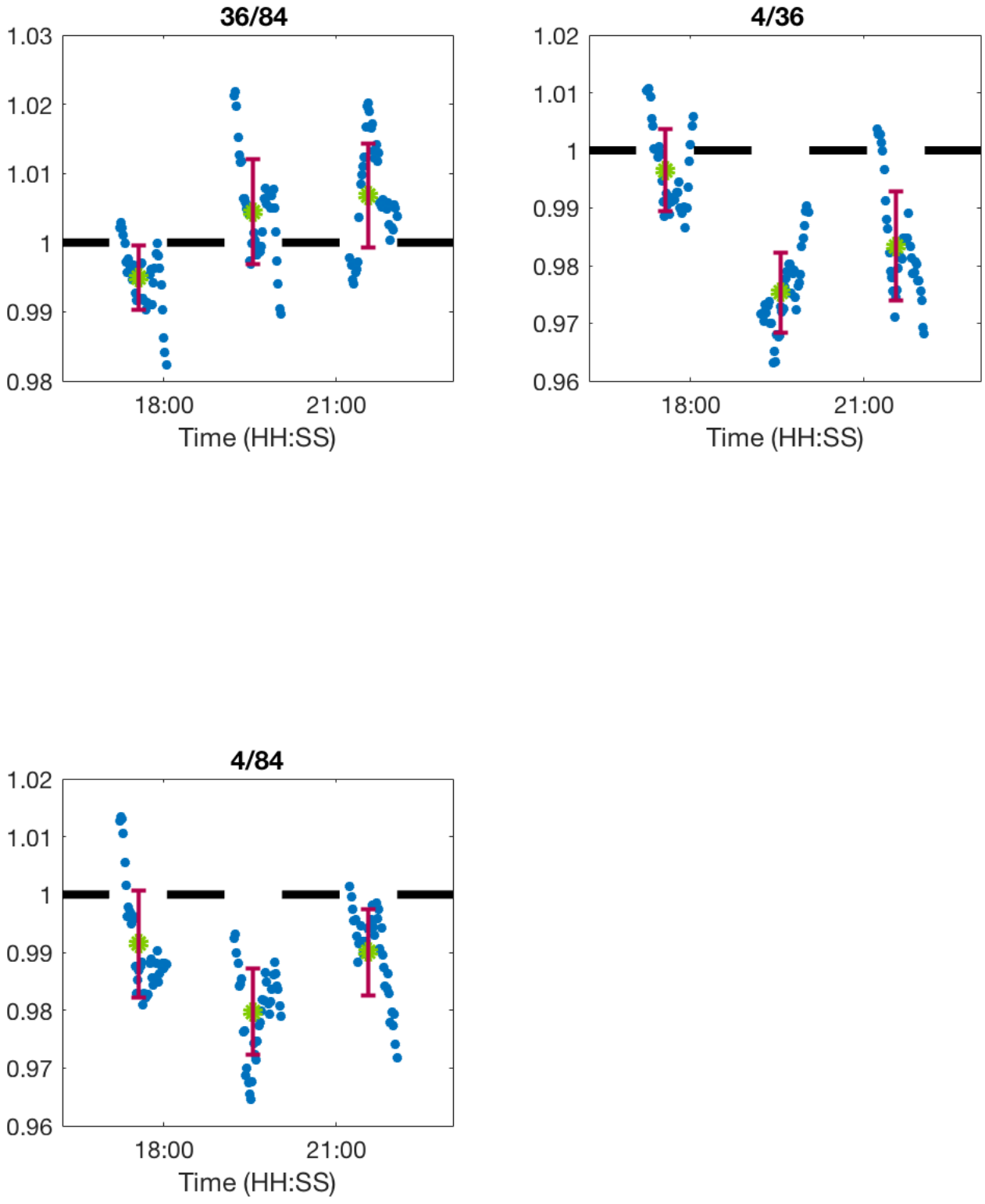

Figure 14: Ratio of the running mean and the interpolated data from the 1/25/18 data during the air-water switching experiment performed overnight with stainless steel capillary in 10°C water. Data are plotted the same way as in Fig. 6.

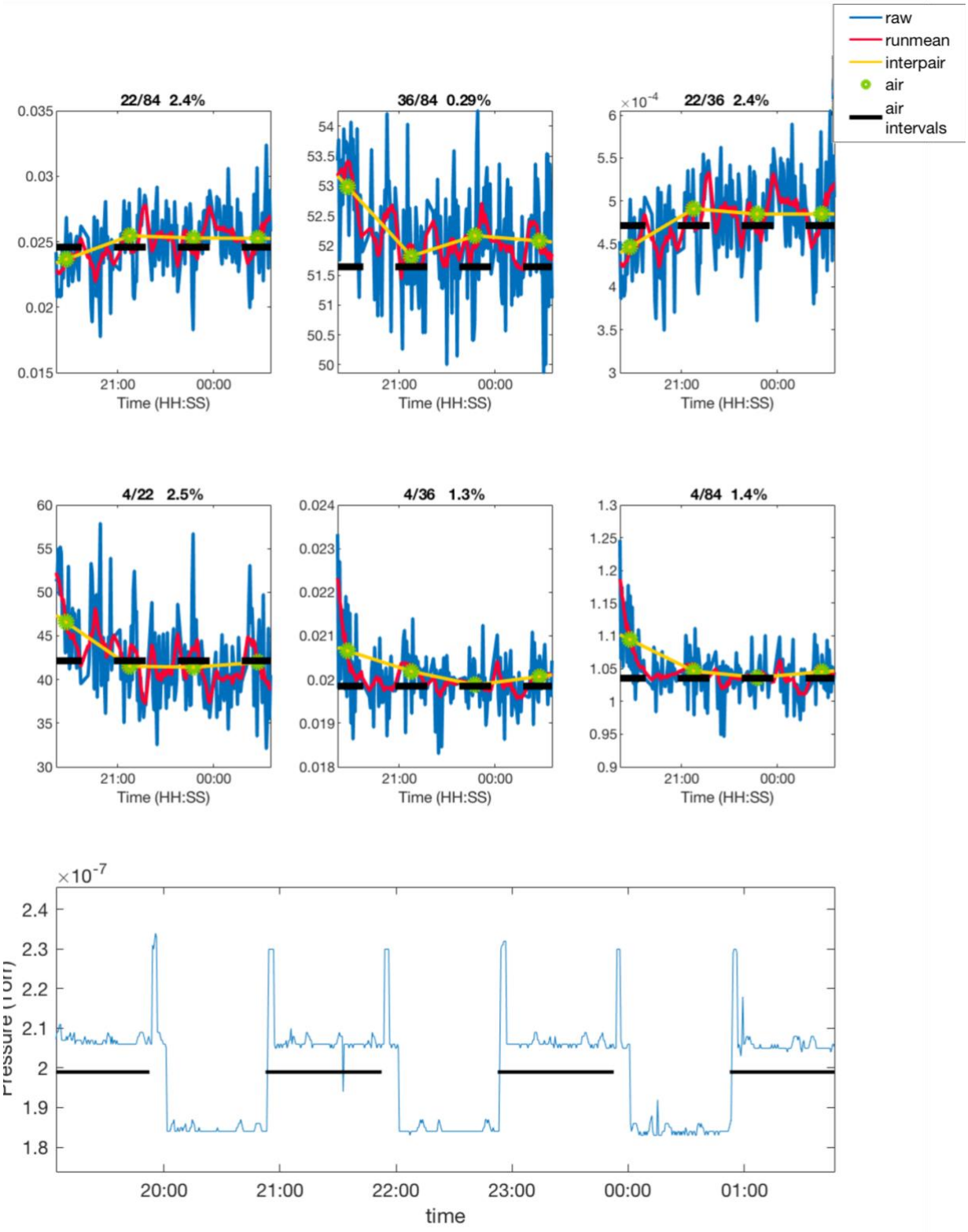

Figure 15: Noble gas ratios for the 1/31/18 air-water switching experiment with stainless steel capillary in 10°C water and a plot of pressure vs. time. Data are plotted in the same way as Fig. 9.

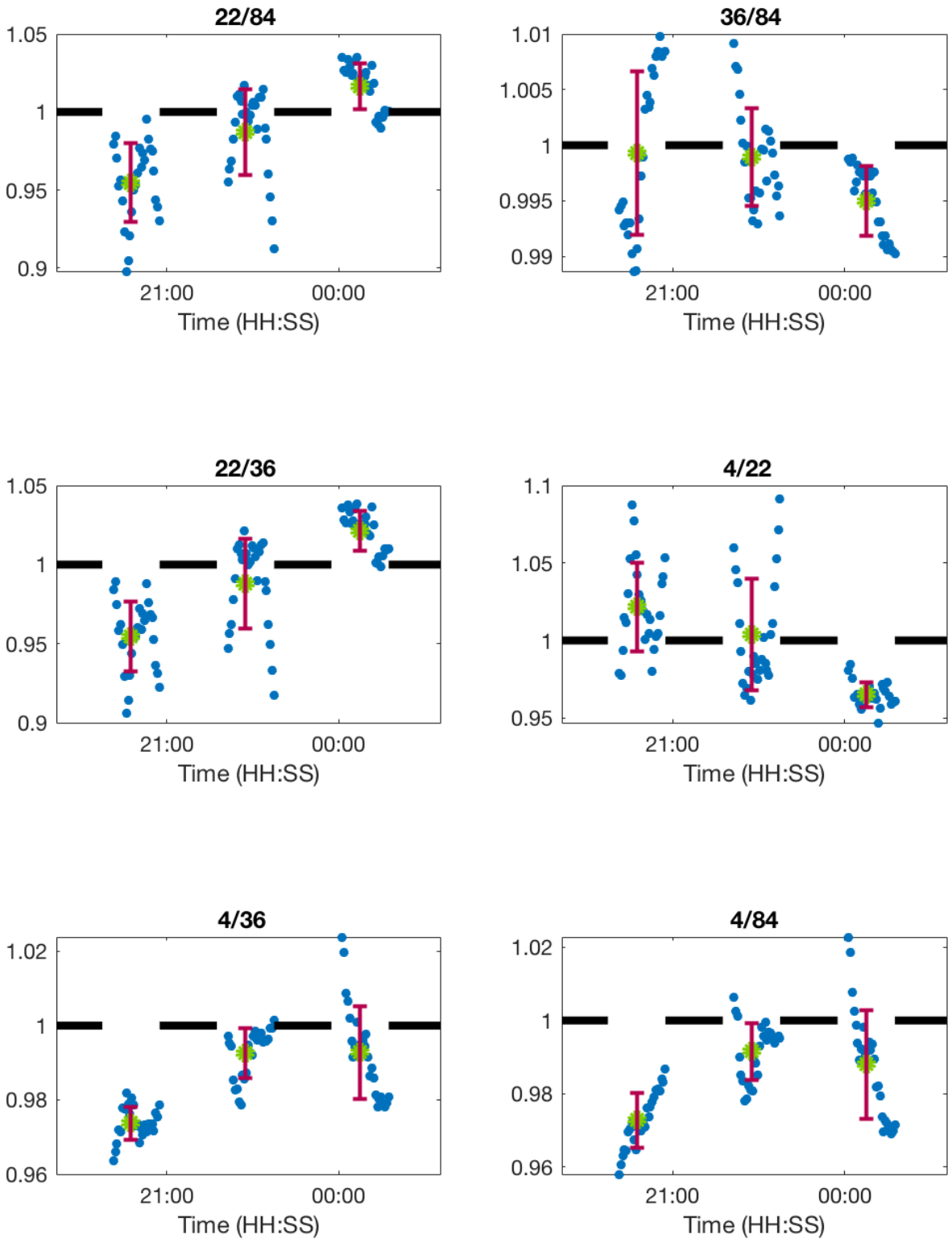

Figure 16: Ratio of the running mean and the interpolated data from the 1/31/18 data during the air-water switching experiment performed overnight with stainless steel capillary in 10°C water. Data are plotted the same way as in Fig. 6.

Starting with the 1/26/18 experiment at 10°C, Ne was measured again as an additional proxy by which to determine whether He was equilibrating. Ne is difficult to equilibrate at low temperatures, but not as difficult as equilibrating He. Thus, if Ne is equilibrating then there is a possibility that He could equilibrate as well. If Ne was not equilibrating, then He would not equilibrate. Experiments at 10°C including Ne showed undersaturation of the Ne and He ratios during the first water interval but improved in subsequent water intervals. Thus, air-water experiments were performed overnight to determine if equilibration of the gases into the headspace would improve with longer experiment durations. Figure 17 and 18 show the results of the overnight experiments, which do not show a significant improvement over experiments with shorter durations. The overnight experiments on 2/8/18 and 2/9/18 showed undersaturation particularly for the He ratios. The air flow of the gas recirculation loop was increased again in an attempt to improve the equilibration. The equilibration improved for the Ne ratios, but did not improve for the He ratios. This suggests that changes to the current configuration rather than adjustments to experimental conditions are needed to improve equilibration.

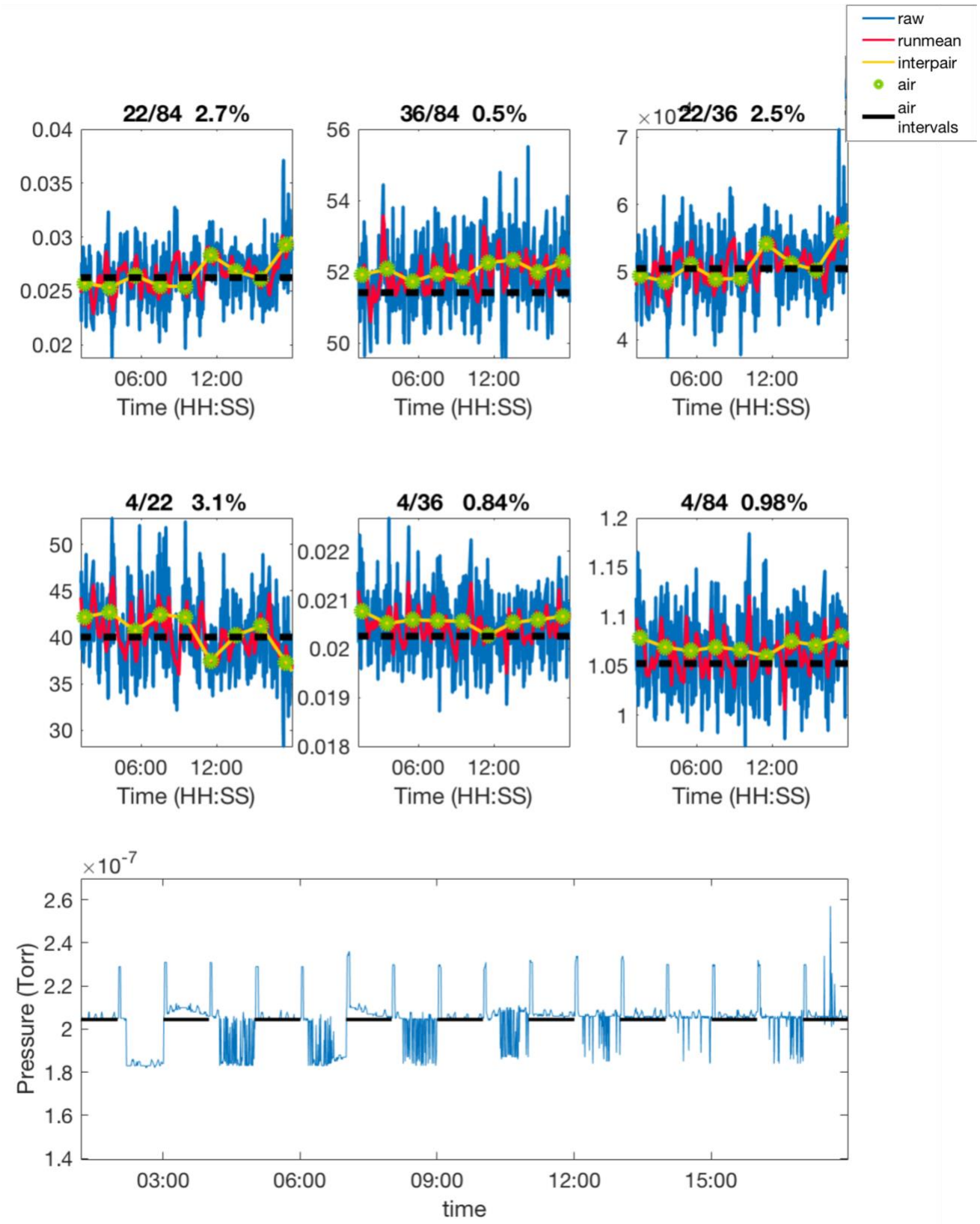

Figure 17: Noble gas ratios for the 2/8/18 air-water switching experiment with 10°C water performed overnight and a plot of pressure vs. time. Data plotted in the same way as Fig. 9.

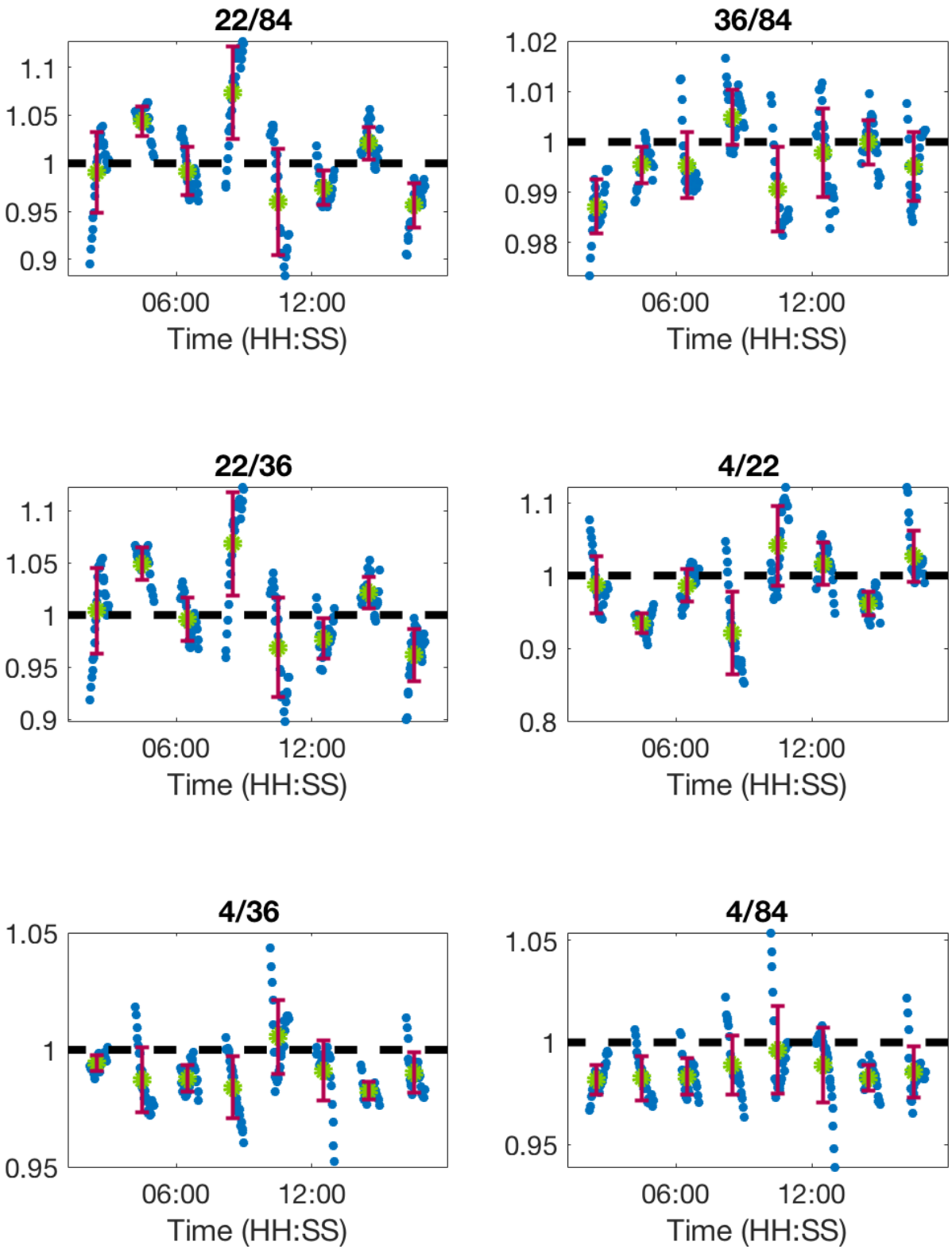

Figure 18: Ratio of the running mean and the interpolated data from the 2/8/18 data during the air-water switching experiment performed overnight with stainless steel capillary in 10°C water. Data are plotted the same way as in Fig. 6.

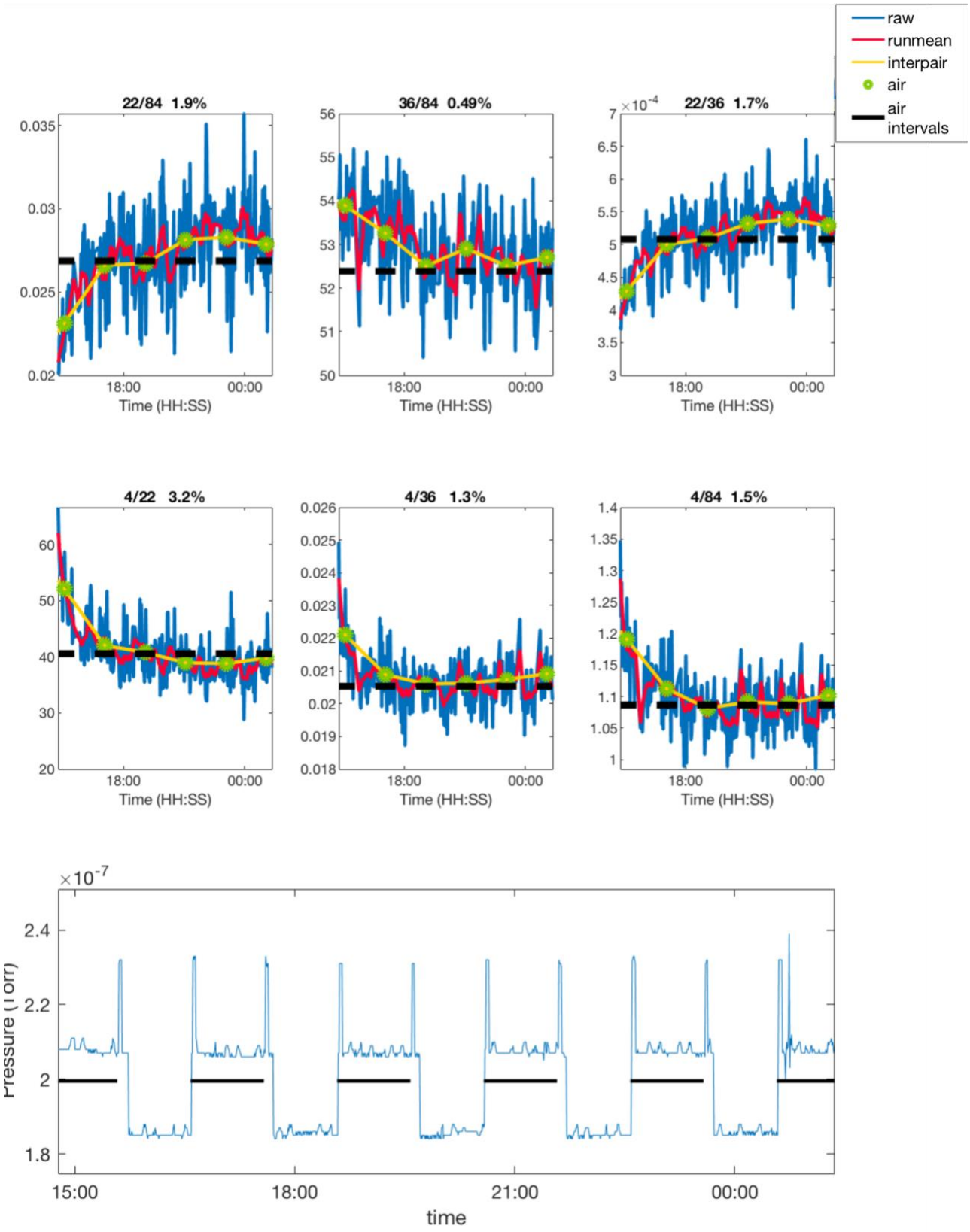

Figure 19: Noble gas ratios for the 2/20/18 air-water switching experiment with 10°C water with a higher air flow rate and a plot of pressure vs. time. Data are plotted in the same way as Fig. 9.

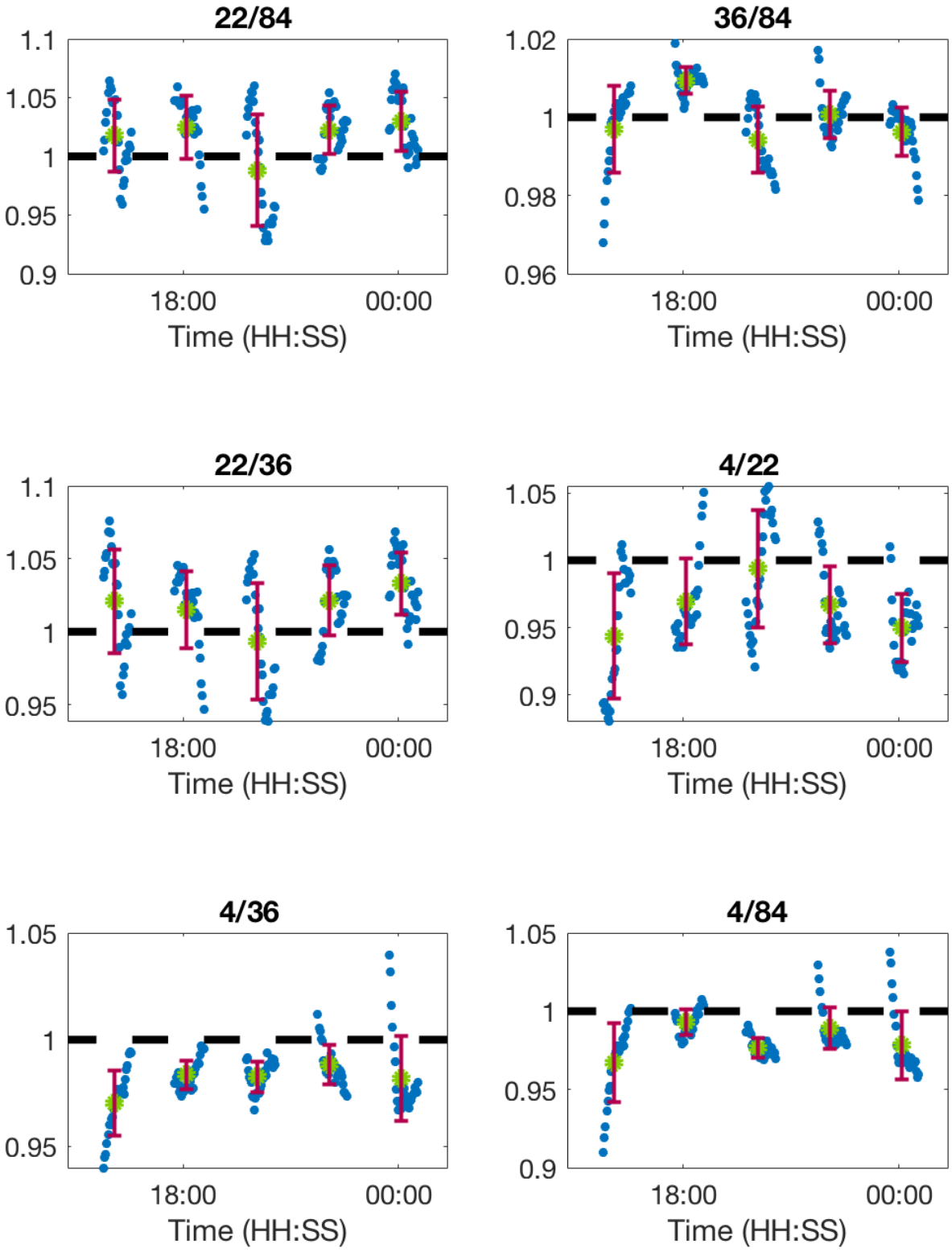

Figure 20: Ratio of the running mean and the interpolated data from the 2/20/18 data during the air-water switching experiment performed with stainless steel capillary in 10°C water with a higher flow rate. Data are plotted the same way as in Fig. 6.

In switching to the stainless steel capillary, pressure fluctuations were primarily observed during water intervals as shown in Figure 13 and 17. In previous experiments, pressure fluctuations were often caused by contaminants in the capillary or uneven edges of the capillary. To remove any contaminants, nitrogen was used to flush the capillary between the VICI valve and the wet side. Subsequent experiments continued to show pressure fluctuations during both the air and water intervals. Both ends of the capillary going to air and going to water were cut in order to smooth out the ends of the capillary. However, we continued to observe pressure fluctuations during both the air and water intervals. Further investigation into this problem will involve flushing the capillary going from the VICI to the inlet valve with nitrogen in order to determine if a contamination exists in the capillary common to both air and water measurements.

Table 10: Precision values for all air-water switching experiments

Date	Ne/Xe	Ar/Xe	Kr/Xe	Ne/Kr	Ar/Kr	Ne/Ar	He/Ne	He/Ar	He/Kr	He/Xe
11/3/18	0.68	0.30	0.32	0.65	0.17	0.59	1.2	0.95	0.91	0.97
11/5/18	0.62	0.42	0.36	0.68	0.23	0.52	2.3	2.3	2.3	2.2
1/15/18					0.36			0.31	0.47	
1/16/18					0.38			0.56	0.56	
1/17/18					0.51			0.54	0.79	
1/18/18					0.55			0.64	0.39	
1/19/18					0.39			0.65	0.68	
1/20/18					0.43			0.54	0.72	
1/23/18					0.48			1.2	1.1	
1/24/18					0.83			1.4	0.91	
1/25/18					0.47			0.90	0.77	
1/26/18				8.6	0.94	7.8	9.1	0.64	0.65	
1/28/18				7.8	0.34	7.4	8.7	0.37	0.57	
1/31/18				2.4	0.29	2.4	2.5	1.3	1.4	
2/1/18				1.8	0.52	1.8	2.2	1.0	1.0	
2/8/18				2.7	0.50	2.5	3.1	0.84	0.98	
2/9/18				2.1	0.55	2.0	2.1	0.82	1.0	
2/20/18				1.9	0.49	1.7	3.2	1.3	1.5	
2/21/18				2.2	0.48	2.0	2.4	1.1	1.2	

In addition to assessing the equilibration of the system, the precision values were compared for all air-water switching experiments. Experiments conducted from 1/15/18 to 1/18/18 were conducted with the same parameters with stainless steel capillary. The experiments conducted with the higher air flow rate on 1/19/18 and 1/20/18 show better precision for Ar/Kr, but worse precision values for the He ratios. The precision for the He ratios worsens after the temperature of the water bath is set to 10°C in the 1/23-25/18 experiments, which was expected since He is more difficult to equilibrate at lower temperatures. The worse precisions for the 1/26/18 and 1/28/18 data may indicate instabilities in the Ne ion current for those experiments since the precision for the He ratios improved from the previous experiments. This is supported by the addition of Ne to the template for measurements on 1/26/18 and the resetting of the filament on 1/28/18. In earlier assessments of the stability of the Ne ion current, we found that the Ne ion current tended to increase and recover after the filament was reset. This could possibly account for the worse precisions for the Ne ratios on 1/26/18 and 1/28/18 and is supported by the relatively better precision values for the Ne ratios in subsequent experiments when the filament was not reset, and a new template was not used. The precision values worsened for Ne ratios when the experiments were conducted overnight and worsened for Ne ratios when the air flow was increased again. These findings suggest that the equilibration method has a significant effect on the precision. This is supported by the change in only the He and Ne ratios between each experiment whereas the precision of Ar/Kr is relatively constant. In addition, the instability of the Ne signal caused by the problems with the mass spectrometer could have impacted the precision of the Ne ratios.

The new configuration of the system is a work-in-progress. The system currently has the benefit of being mostly leak-proof to He, allowing for measurements of He and showing steady

ratios and thus, relatively good precision. Given the limitations of the quadrupole mass spectrometer at the time the experiments were made, the actual precision of this method is probably much better than assessed here. However, the current configuration is not sufficiently equilibrating at colder temperatures and shows significant pressure fluctuations which may have an effect on the noble gas ratios. Increasing the flow rate through the gas recirculation loop and increasing the duration of the experiments did not significantly improve the equilibration. Further attempts to improve the equilibration would include lengthening the capillary in order to reduce the flow rate out of the headspace. In addition, the source of the pressure fluctuations is currently unknown and requires further investigation.

Chapter 4: Conclusions

The objective of this project was to adapt the previous mass spectrometer system developed by Manning et al. to measure He in addition to the other noble gases. The precisions of the instrument in the old configuration and various experimental conditions in the new configuration were calculated and compared. The equilibration of both systems was compared and leak tests with He were done on both systems.

Analysis of the performance of the new system has shown that the system is a work-in-progress. The new configuration of the system is capable of measuring He at 22°C with precision values better than 0.65% for He/Ar and 0.80% for He/Xe. In comparison, the discrete mass spectrometer system by Visser et al. measured He with a precision of 2.1% and the continuous mass spectrometer system developed by Mächler et al. measured He with a precision of 3.0%.[38,43]

Further challenges remain with measuring He at temperatures of 10°C and below. With water at 10°C, ratios containing He and Ne show undersaturation and incomplete equilibration. Further experiments will need to be done for water bath temperatures between 10°C and 22°C to quantify the working range of the system. In addition, further attempts to improve equilibration can be done by lengthening the capillary to reduce the air flow rate out of the headspace of the equilibrator cartridge. An alternative method of improving the equilibration could involve using a custom-made stainless steel capillary with an inner diameter equal to that of the fused silica capillary. However, this route would be very costly and make it more difficult for replication of our system. Another alternative method would be to modify the use of the equilibration cartridge itself. Currently, the headspace of the equilibrator cartridge is evacuated to promote the transfer of gases from the water into the headspace. A possible modification could be to introduce a

sweep gas, such as N_2, into the lumens of the membrane contractor in a direction counter to the flow of water. This has the effect of disturbing the equilibrium of the gas and water phases and physically forcing more gas into the headspace. [44] The sweep-gas method can be coupled with the vacuum method in order to increase the amount of gas extracted from the water, and could improve the equilibration of He and Ne.

Additionally, because difficulties with the mass spectrometer affected the amplitude of the signal, further experiments will be performed after the mass spectrometer is sent to Hiden for repairs. Once the signal strength is recovered, the entire suite of noble gases, including Xe, can be measured. Measuring Xe will allow for better assessment of how the system is equilibrating. Currently, Ar/Kr is the only noble gas ratio being assessed that does not include He and Ne. By including Xe in the measurements, we can better assess whether issues with the precision are due to the equilibration or due to inconsistencies in the mass spectrometer itself.

Although there are difficulties with the equilibration method, helium leak tests have shown that the system is leak-tight to He relative to the old configuration. To support these findings, an additional He leak test can be performed on the system in which the wet side of the equilibration system is isolated with a bag that is mostly impermeable to He and to flow He into the bag. Performing this leak test would allow us to quantify if there is significant He leakage into the system when He is increasing in the environment rather than being specifically targeted at a certain component. Careful leak-testing of the system will be useful for future experiments to determine what type of materials can be used when He and other diffusive gases need to be measured.

The current configuration of the system can effectively measure He at temperatures at 22°C and above. The results of this project can be applied this summer at experiments performed

at the SUSTAIN wind-wave tank in Miami. Measuring helium will allow for better parametrization of the effect of bubble processes on air-sea gas exchange. In addition, our system could potentially be applied to study the residence times of groundwater and help quantify the amount of oxygen in groundwater resulting from air injection. Although further optimization of the system is needed to expand the working range of the instrument, we have developed a system capable of measuring He with good precision at higher temperatures.

References

1. Burnard, P.; Zimmermann, L.; Sano, Y., The Noble Gases as Geochemical Tracers: History and Background. In *The Noble Gases as Geochemical Tracers*, Burnard, P., Ed. Springer Berlin Heidelberg: Berlin, Heidelberg, 2013; pp 1-15.

2. Aeschbach-Hertig, W.; Peeters, F.; Beyerle, U.; Kipfer, R., Interpretation of dissolved atmospheric noble gases in natural waters. *Water Resources Research* **1999,** *35* (9), 2779-2792.

3. Ozima, M.; Podosek, F. A., *Noble Gas Geochemistry*. Cambridge University Press: Cambridge, UNITED KINGDOM, 2001.

4. Stanley, R. H. R.; Jenkins, W. J., Noble Gases in Seawater as Tracers for Physical and Biogeochemical Ocean Processes. In *The Noble Gases as Geochemical Tracers*, Burnard, P., Ed. Springer-Verlag Berlin Heidelberg: 2013; pp 55-79.

5. Jähne, B.; Heinz, G.; Dietrich, W., Measurement of the diffusion coefficients of sparingly soluble gases in water. *Journal of Geophysical Research: Oceans* **1987,** *92* (C10), 10767-10776.

6. Manning, C. C.; Stanley, R. H. R.; Nicholson, D. P.; Squibb, M. E., Quantifying air-sea gas exchange using noble gases in a coastal upwelling zone. *IOP Conference Series: Earth and Environmental Science* **2016,** *35* (1), 012017.

7. Brennwald, M. S.; Vogel, N.; Scheidegger, Y.; Tomonaga, Y.; Livingstone, D. M.; Kipfer, R., Noble Gases as Environmental Tracers in Sediment Porewaters and Stalagmite Fluid Inclusions. In *The Noble Gases as Geochemical Tracers*, Burnard, P., Ed. Springer Berlin Heidelberg: Berlin, Heidelberg, 2013; pp 123-153.

8. Kipfer, R.; Aeschbach-Hertig, W.; Peeters, F.; Stute, M., *Noble Gases in Lakes and Ground Waters*. 2002; Vol. 47.

9. Craig, H.; Weiss, R. F., Dissolved gas saturation anomalies and excess helium in the ocean. *Earth and Planetary Science Letters* **1971,** *10* (3), 289-296.

10. Keeling, R. F., On the role of large bubbles in air-sea gas exchange and supersaturation in the ocean. *Journal of Marine Research* **1993,** *51* (2), 237-271.

11. Liang, J.-H.; Deutsch, C.; McWilliams, J. C.; Baschek, B.; Sullivan, P. P.; Chiba, D., Parameterizing bubble-mediated air-sea gas exchange and its effect on ocean ventilation. *Global Biogeochemical Cycles* **2013,** *27* (3), 894-905.

12. Thorpe, S. A., A Model of the Turbulent Diffusion of Bubbles below the Sea Surface. *Journal of Physical Oceanography* **1984,** *14* (5), 841-854.

13. Stanley, R. H.; Jenkins, W. J.; Lott, D. E.; Doney, S. C., Noble gas constraints on air-sea gas exchange and bubble fluxes. *Journal of Geophysical Research: Oceans* **2009,** *114* (C11).

14. Hamme, R. C.; Emerson, S. R.; Severinghaus, J. P.; Long, M. C.; Yashayaev, I., Using Noble Gas Measurements to Derive Air-Sea Process Information and Predict Physical Gas Saturations. *Geophysical Research Letters* **2017,** *44* (19), 9901-9909.

15. Hamme, R. C.; Emerson, S. R., Constraining bubble dynamics and mixing with dissolved gases: Implications for productivity measurements by oxygen mass balance. *Journal of Marine Research* **2006,** *64* (1), 73-95.

16. Blomquist, B. W.; Brumer, S. E.; Fairall, C. W.; Huebert, B. J.; Zappa, C. J.; Brooks, I. M.; Yang, M.; Bariteau, L.; Prytherch, J.; Hare, J. E.; Czerski, H.; Matei, A.; Pascal, R. W., Wind Speed and Sea State Dependencies of Air-Sea Gas Transfer: Results From the High Wind Speed Gas Exchange Study (HiWinGS). *Journal of Geophysical Research: Oceans* **2017,** *122* (10), 8034-8062.

17. Woolf, D. K.; Thorpe, S. A., Bubbles and the air-sea exchange of gases in near-saturation conditions. *Journal of Marine Research* **1991,** *49* (3), 435-466.

18. Spitzer, W. S.; Jenkins, W. J., Rates of vertical mixing, gas exchange and new production: Estimates from seasonal gas cycles in the upper ocean near Bermuda. *Journal of Marine Research* **1989,** *47* (1), 169-196.

19. Hood, E. M.; Howes, B. L.; Jenkins, W. J., Dissolved gas dynamics in perennially ice-covered Lake Fryxell, Antarctica. *Limnology and Oceanography* **1998,** *43* (2), 265-272.

20. Loose, B.; Jenkins, W. J., The five stable noble gases are sensitive unambiguous tracers of glacial meltwater. *Geophysical Research Letters* **2014,** *41* (8), 2835-2841.

21. Jacobs, S. S.; Helmer, H. H.; Doake, C. S. M.; Jenkins, A.; Frolich, R. M., Melting of ice shelves and the mass balance of Antarctica. *Journal of Glaciology* **1992,** *38* (130), 375-387.

22. Schlosser, P., *Helium: A new tracer in Antarctic Oceanography*. 1986; Vol. 321, p 233-235.

23. Mamyrin, B. A.; Tolstikhin, L. N., Chapter 9 - Helium Isotopes in Seawater. In *Developments in Geochemistry*, Elsevier: 1984; Vol. Volume 3, pp 193-202.

24. Schlosser, P.; Winckler, G., Noble Gases in Ocean Waters and Sediments. *Reviews in Mineralogy and Geochemistry* **2002,** *47* (1), 701-730.

25. Beyerle, U.; Aeschbach-Hertig, W.; Imboden, D. M.; Baur, H.; Graf, T.; Kipfer, R., A Mass Spectrometric System for the Analysis of Noble Gases and Tritium from Water Samples. *Environmental Science & Technology* **2000,** *34* (10), 2042-2050.

26. Graham, D. W., Noble Gas Isotope Geochemistry of Mid-Ocean Ridge and Ocean Island Basalts: Characterization of Mantle Source Reservoirs. *Reviews in Mineralogy and Geochemistry* **2002,** *47* (1), 247-317.

27. Tomonaga, Y.; Marzocchi, R.; Pera, S.; Pfeifer, H.-R.; Kipfer, R.; Decrouy, L.; Vennemann, T., Using noble-gas and stable-isotope data to determine groundwater origin and flow regimes: Application to the Ceneri Base Tunnel (Switzerland). *Journal of Hydrology* **2017,** *545*, 395-409.

28. Tomonaga, Y.; Brennwald, M. S.; Kipfer, R., Using helium and other noble gases in ocean sediments to characterize active methane seepage off the coast of New Zealand. *Marine Geology* **2013,** *344*, 34-40.

29. Holzner, C. P.; McGinnis, D. F.; Schubert, C. J.; Kipfer, R.; Imboden, D. M., Noble gas anomalies related to high-intensity methane gas seeps in the Black Sea. *Earth and Planetary Science Letters* **2008,** *265* (3), 396-409.

30. Aeschbach-Hertig, W.; Solomon, D. K., Noble Gas Thermometry in Groundwater Hydrology. In *The Noble Gases as Geochemical Tracers*, Burnard, P., Ed. Springer Berlin Heidelberg: Berlin, Heidelberg, 2013; pp 81-122.

31. Emerson, S.; Stump, C.; Wilbur, D.; Quay, P., Accurate measurement of O2, N2, and Ar gases in water and the solubility of N2. *Marine Chemistry* **1999,** *64* (4), 337-347.

32. Stanley, R. H. R.; Baschek, B.; Lott, D. E.; Jenkins, W. J., A new automated method for measuring noble gases and their isotopic ratios in water samples. *Geochemistry, Geophysics, Geosystems* **2009,** *10* (5), n/a-n/a.

33. D.E. Lott, I.; Jenkins, W. J., Advances in Analysis and Shipboard Processing of Tritium and Helium Samples. *International WOCE Newsletter* **1998,** (30), 27-30.

34. Sano, Y.; Takahata, N., Measurement of Noble Gas Solubility in Seawater Using a Quadrupole Mass Spectrometer. *Journal of Oceanography* **2005,** *61* (3), 465-473.

35. Manning, C. C.; Stanley, R. H. R.; Lott, D. E., Continuous Measurements of Dissolved Ne, Ar, Kr, and Xe Ratios with a Field-Deployable Gas Equilibration Mass Spectrometer. *Analytical Chemistry* **2016,** *88* (6), 3040-3048.

36. Tortell, P. D., Dissolved gas measurements in oceanic waters made by membrane inlet mass spectrometry. *Limnology and Oceanography: Methods* **2005,** *3* (1), 24-37.

37. Visser, A.; Singleton, M. J.; Hillegonds, D. J.; Velsko, C. A.; Moran, J. E.; Esser, B. K., California GAMA Special Study: Noble Gas Membrane Inlet Mass Spectrometry: A Rapid, Low-Cost Method to
Determine Travel Times at Recharge Operations Using Noble Gas Tracers. *Lawrence Livermore National Laboratory LLNL-TR-548931* **2011**, 41.

38. Mächler, L.; Brennwald, M. S.; Kipfer, R., Membrane Inlet Mass Spectrometer for the Quasi-Continuous On-Site Analysis of Dissolved Gases in Groundwater. *Environmental Science & Technology* **2012,** *46* (15), 8288-8296.

39. Mächler, L.; Brennwald, M. S.; Tyroller, L.; Livingstone, D. M.; Kipfer, R., Conquering the Outdoors with On-site Mass Spectrometry. *CHIMIA International Journal for Chemistry* **2014,** *68* (3), 155-159.

40. Design & Operating Guidelines for Liqui-Cel® Extra-Flow Membrane Contactors. http://www.liquicel.com/uploads/documents/Operating_Procedure_OP151_Rev19%204-20-16%20_ke.pdf.

41. Wang, R.; Zhang, H. Y.; Feron, P. H. M.; Liang, D. T., Influence of membrane wetting on CO2 capture in microporous hollow fiber membrane contactors. *Separation and Purification Technology* **2005,** *46* (1), 33-40.

42. Cassar, N.; Barnett, B. A.; Bender, M. L.; Kaiser, J.; Hamme, R. C.; Tilbrook, B., Continuous High-Frequency Dissolved O2/Ar Measurements by Equilibrator Inlet Mass Spectrometry. *Analytical Chemistry* **2009,** *81* (5), 1855-1864.

43. Visser, A.; Singleton, M. J.; Hillegonds, D. J.; Velsko, C. A.; Moran, J. E.; Esser, B. K., A membrane inlet mass spectrometry system for noble gases at natural abundances in gas and water samples. *Rapid Communications in Mass Spectrometry* **2013,** *27* (21), 2472-2482.

44. McLeod, A.; Jefferson, B.; McAdam, E. J., Toward gas-phase controlled mass transfer in micro-porous membrane contactors for recovery and concentration of dissolved methane in the gas phase. *Journal of Membrane Science* **2016,** *510*, 466-471.